Ore Geology Reviews 143 (2022) 104769

Contents lists available at ScienceDirect

Ore Geology Reviews

journal homepage: www.elsevier.com/locate/oregeorev

Isotopic constraints on the age and source of ore-forming fluids of the Bou Azzer arsenide ores (Morocco)

I. Subías [a,1], I. Fanlo [a,*], Z. Hajjar [b,d], F. Gervilla [b,c], K. Billström [e]

[a] Dpto. Ciencias de la Tierra, Universidad de Zaragoza, c/ Pedro Cerbuna 12 (Edificio Geológicas), 50009 Zaragoza, Spain
[b] Departamento de Mineralogía y Petrología, Universidad de Granada, Avda. Fuentenueva s/n, 18071 Granada, Spain
[c] Instituto Andaluz de Ciencias de la Tierra (UGR-CSIC), Avda. Palmeras 4, Armillas 18100 Granada, Spain
[d] Laboratoire Geosciences, Eau et Environement (L-G2E), Faculté des Sciences de Rabat, Université Mohammed V, Rabat, Morocco
[e] Department of Geological Sciences, Swedish Museum of Natural History, Frescativagen 40, Box 50007, SE-104 05 Stockholm, Sweden

ARTICLE INFO

Keywords:
Co-Ni arsenide ores
Hydrothermal arsenides
Pb
Rb/Sr
Sm/Nd and S isotopes
Bou Azzer

ABSTRACT

The Bou Azzer district in Morocco has a long mining history since the beginning of the XXst century during which it has become the only world producer of Co from primary, hydrothermal Co arsenide ores. Orebodies are structurally controlled, and mainly distributed along fault contacts between Cryogenian ophiolite-related serpentinite bodies and intrusive quartz diorite or, locally, ophiolitic gabbros or Ediacaran volcanic rocks. Ore formation took place through a multi-stage mineralizing process that included an early stage composed by gold, quartz, chlorite, muscovite and calcite, followed by the main arsenide and sulfarsenide stage (subdivided into three substages, IIa: Ni-rich, Co ores, IIb: Co-Fe ores and IIc: Fe-Co ores), and ending with an epithermal stage characterized by the precipitation of sulfides along with quartz and calcite. Field relations and most previous geochronologic dating pointed to a post Pan-African age of ore formation, mainly coincident with the Hercynian orogeny.

The isotopic study presented in this paper includes S, Pb, Rb/Sr and Sm/Nd data of a set of ore mineral samples from three deposits (Aghbar, Tamdrost and Aït Ahmane), as well as of regional samples representative of the different lithologies occurring in the Bou Azzer area. The isotope data set was completed with S isotope analyses of arsenide and sulfarsenide minerals from five ore deposits (Filon 7/5, Aghbar, Tamdrost, Ightem and Aït-Ahmane) and of some whole-rock regional samples. Results show that ores formed during multi-episodic hydrothermal events connected with hercynian reactivation of Devonian-Carboniferous faults, supporting previous geochronologic dating. The obtained Pb, Sr, Nd and S isotopic signatures of ore minerals and regional rocks further show that ophiolite-related lithologies became isotopically modified by interaction with crustal material and afterwards acted as the main source of ore-forming elements. Nevertheless, isotopic data do not fully concur with such a simple scenario but are quite consistent with a rather complex interpretation based on multi-source origin of some elements and isotopes scavenged from a number of isotopically different lithologies both from the inferred basement and the volcanic and sedimentary cover.

1. Introduction

Most cobalt production in the world comes from sediment-hosted copper deposits, magmatic Ni-Cu ores, five-element hydrothermal veins and laterite deposits, as a by-product. However, the Bou Azzer district in Morocco is nowadays the only locality in the world where cobalt is mined directly from Co-rich arsenide and sulfarsenide minerals as a primary ore. This world-class mining district includes more than 100 occurrences of Co-arsenide ores (Leblanc and Billaud, 1982) corresponding to more than 2% of the world's cobalt production (U.S. Geological Survey, 2013). Currently, the mean annual production is about 150,000 t of ore (Ikenne et al., 2020) at an average grade of 1% Co and 1% Ni. In addition to Co and Ni, 3–4 g/t gold and silver are also recovered as by-products (Bouabdellah et al., 2016).

As a consequence of its huge economic potential, the district has been extensively studied over the last few decades, which has resulted in the

* Corresponding author.
E-mail address: fanlo@unizar.es (I. Fanlo).
[1] In memorian.

https://doi.org/10.1016/j.oregeorev.2022.104769
Received 15 March 2021; Received in revised form 24 January 2022; Accepted 8 February 2022
Available online 14 February 2022

release of research papers, theses, and unpublished mining company reports. In spite of the abundant literature, uncertainties still remain on the nature of mineral assemblages and paragenetic sequences (En-Naciri, 1995, Dolansky, 2007, Ahmed et al., 2009, Gervilla et al., 2012, Lasobras, 2012, Lázaro, 2012, Maacha, 2013, Bouabdellah et al., 2016, Ikenne et al., 2020), the physicochemical characteristics of ore-forming fluids (En-Naciri, 1995, Essarraj et al., 2005, Dolansky, 2007) and the timing of ore formation relative to the main tectonic events in the region (Clauer, 1976, Leblanc and Billaud, 1982, Gasquet et al., 2005, Dolansky, 2007, Oberthür et al., 2009, Blein et al., 2014, Bouabdellah et al., 2016, Tourneur et al., 2021).

Thus, the aim of this paper is to shed some light on the formation age of the Co-Ni arsenide ores of the Bou Azzer district as well as on the provenance of ore-forming fluids by means of a Pb, Sr, Nd and S isotope survey on a representative set of samples from different ore deposits and regional lithological units.

2. Geology and ore deposits of the Bou Azzer district

The Moroccan Anti-Atlas belt, separated from the High Atlas to the North by the South Atlas Fault, is constituted by several inliers of Precambrian units within Late Ediacaran and younger units (Álvaro et al., 2014, Soulaimani et al, 2018; Table 1). One of these inliers, the Bou Azzer-El Grâara inlier (Fig. 1) is structurally the most complex portion of the whole Anti-Atlas (Leblanc, 1981). The oldest formation located in the south-eastern part of the Bou Azzer inlier is made up of gneisses, pegmatites, schists, tholeiitic basalts, quartzites and carbonates. Such basement lithologies have been assigned to a Paleoproterozoic suite of rocks by Leblanc (1981); however, new U-Pb dating data for rocks gathered under the name Tachdamt Bleida group, and Tazegzaout group in Bou Azzer demonstrate Tonian and Early Cryogenian ages (900–700 Ma; Clauer, 1976, D'Lemos et al., 2006, Blein et al., 2014, Hefferan et al., 2014, Bouougri et al., 2020, Triantafyllou et al., 2020). In the North East Bou Azzer inlier outcrop a complex tectonic assemblage made up of metagreywackes and arc-related basalts, andesites, rhyolites and tuffs has been grouped under the name Tichinbanine Ben Lagrad group, and dated between 761 ± 7 Ma and 767 ± 7 Ma (Blein et al., 2014, Triantafyllou et al., 2018, 2020). An important Cryogenian terrane is defined by the Bou Azzer Group, which includes a mafic–ultramafic complex (serpentinized peridotites containing podiform chromitites, layered gabbros, pillow lavas, diabase dykes and associated sedimentary rocks), interpreted by Leblanc (1981) as an ophiolite sequence. The above formations were intruded by syn- to post-kinematic stocks: *syn*-orogenic (640–660 Ma) quartz-diorite (Mrini, 1993, Samson et al., 2004, Inglis et al., 2003, El Hadi et al., 2010, Blein et al., 2014, Triantafyllou et al., 2020) and post-orogenic (594 ± 1.2 Ma) gabbrodiorite (Inglis et al., 2004, Blein et al., 2014). All the above formations were thrusted and folded during the Pan-African orogeny and were unconformably overlain by the molassic Tiddiline Group, the Ediacaran volcanoclastic pile (e.g. ignimbrites, andesites, conglomerates, sandstones dated at 606 ± 5 Ma; Blein et al., 2014), the Ouarzazate Supergroup (567 ± 5 Ma and 566 ± 4 Ma; Blein et al., 2014) and the lower Cambrian Taroudant Group (541 ± 6 Ma; Blein et al., 2014). According to Gasquet et al. (2005) a regional N–S shortening that occurred during the Variscan orogeny reactivated the major Pan-African faults.

Most Co–Ni–Fe arsenide (±Au ± Ag) deposits are structurally controlled and distributed along the boundaries of the serpentinite massifs which display vertical contacts with the quartz diorites and locally Ediacaran volcanic rocks of the Ouarzazate Group (Tourneur et al., 2021). From the west to the east (Fig. 1), the studied deposits are: Mechoui, Filon 7/5, Aghbar, Tamdrost, Ambed, Ightem, Agoudal, and Aït-Ahmane. Co-Ni-Fe ores in the Bou Azzer inlier display variable shapes: *trans*-tensional, sub-vertical fault-jogs, flame-shaped orebodies, flat lensoidal and pocket-like masses, lodes, veins, veinlets, cemented breccias within veins, and fillings. Further, ores occur in various settings as: i) veins and lodes with sharp wall-rocks along the contacts between serpentinites and other rocks. Locally, arsenide mineralization may extend into serpentinite and quartz diorite wall rocks for 10 m or more (En-Naciri, 1995, Levresse, 2001, El Ghorfi, 2006, Dolansky, 2007, Maacha, 2013, Tourneur et al., 2021); ii) veins and irregular replacement bodies hosted by serpentinites with diffuse, gradational contacts with the host (Hajjar et al. 2021); iii) mineralized veins secant to this contact, hosted mainly in quartz-diorite and rhyolite from the Ouarzazate group (En-Naciri, 1995, Levresse, 2001, El Ghorfi, 2006, Dolansky, 2007, Maacha, 2013, Tourneur et al., 2021). The mineralized structures of the Bou Azzer cobalt district can be grouped into four main directions. E-W, NE-SW, NW-SE and N-S. No consistent paragenetic sequence can be defined owing to multiple overlapping pulses of mineralization; nevertheless, according to Maacha (2013) and Bouabdellah et al. (2016) the sequence of mineral deposition shows three main stages: (I) the early pre-arsenide stage composed by gold, quartz, chlorite, muscovite and calcite, (II) the Co–, Ni-, Fe-rich main arsenide and sulfarsenide stage and (III) an epithermal stage marked by the precipitation of sulfides

Table 1
Rock samples age according to the geochronologic dating of the host formations.

Rock Sample	Rock Type/Ores	Localization	Group	Age Ma	Reference
AgE-1	Andesitic tuffs	Aghbar (PIII)	Ouarzazate	Ediacarian 567 ± 5	Blein et al., 2014
Tiddiline	Sandstone	Near Aït Ahmane	Tidilline	606 ± 14	Blein et al., 2014
WBW2	Granodiorite	Bleida Far West		594 ± 1.2	Inglis et al., 2004
				Upper Cryogenian	
Q Diorite	Quarzt-diorite	Filon 7/5		640–660	Blein et al., 2014; Triantafyllou et al., 2020;
Q Di-6	Quarzt-diorite	Aït Ahmane		640–660	Inglis et al., 2003; Mrini, 1993
Rodingite	Rodingite	Filon 7/5			
OPH-Ga2	Gabbro	Aït Ahmane	Bou Azzer El Grara	697 ± 8	El Hadi et al., 2010
B1, serp.	Serpentinite	Bouismas	Bou Azzer El Grara		
cpx, cumulates	Clinopyroxenite	Aït Ahmane	Bou Azzer El Grara		
OPH-cpx3	Clinopyroxenite	Aït Ahmane	Bou Azzer El Grara		
OPH-DUN 4	Dunite	Aït Ahmane	Bou Azzer El Grara		
OPH-CR1	Chromitite	Aït Ahmane	Bou Azzer El Grara		
				Tonian to Lower Cryogenian	
T Pegm	Pegmatite veins	Ouest Bou Azzer	Tazegzaout	702 ± 5, 695 ± 7	Blein et al., 2014
T ORGN	Orthogneiss	Bleida Far West	Tazegzaout	753 ± 2; 755 ± 9	D'Lemos et al., 2006; Blein et al., 2014
TAK-2a	Rhyolite	Bleida Far West	Tichibanine	767 ± 7	Blein et al., 2014; Triantafyllou et al., 2020
Trh 40	Rhyolite	Bleida Far West	Tichibanine	767 ± 7	Blein et al., 2014
BW-3	Volcanosediments	Bleida Far West	Tichibanine	767 ± 7	Blein et al., 2014
FW-3	Volcanosediments	Bleida Far West	Tichibanine	767 ± 7	Blein et al., 2014
DOL WB	Dolomite	Bleida Far West	Tachdamt-Bleida	789 ± 10	Clauer, 1976

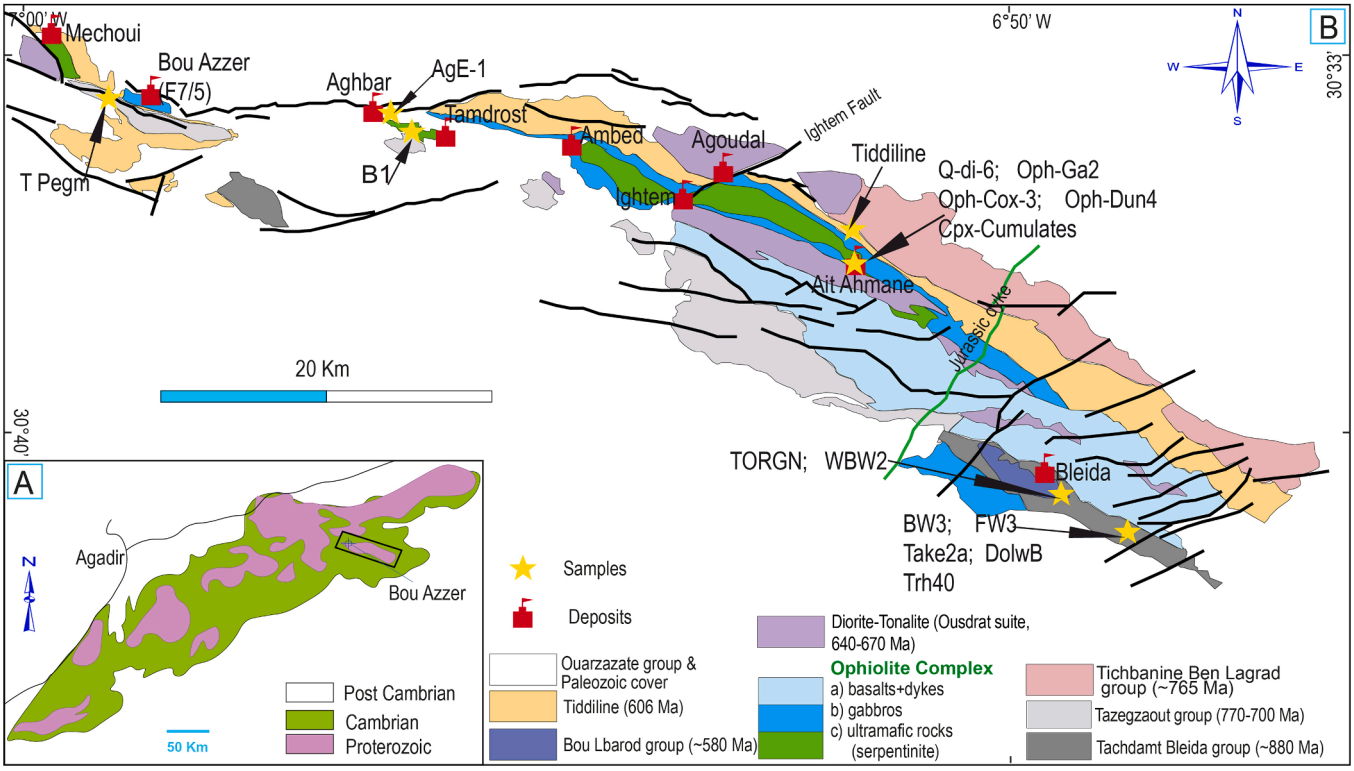

Fig. 1. (A). Simplified geological map of the Anti-Atlas belt. (B). Geological map of Bou Azzer inlier (Central Anti Atlas, Morocco) (modified from Soulaimani et al., 2018), showing the main Co-Ni deposit in the district.

associated to late quartz and calcite. Mineralogy and micro-textures of stage II (En-Naciri, 1995, Dolansky, 2007, Ahmed et al., 2009, Gervilla et al., 2012, Lasobras, 2012, Lázaro, 2012) allow a subdivision into three sub-stages (Fig. 2): (IIa) precipitation of arsenide ores starting with the formation of Ni-rich ores including nickeline, rammelsbergite, Ni-rich skutterudite, members of the rammelsbergite-safflorite-löllingite solid solution series and sulfarsenides (gersdorffite and minor cobaltite), (IIb) formation of Co-Fe rich ore assemblages made up of Co-rich skutterudite, Co-Ni-Fe diarsenides deeply evolving from Co– and Ni-rich compositions to the löllingite corner of the rammelsbergite-safflorite-löllingite ternary system, members of the safflorite-löllingite solid solution series and cobaltite, and (IIc) precipitation of Fe-Co rich ores composed of a third generation of skutterudite, safflorite, löllingite, cobaltite, alloclasite, arsenopyrite and molybdenite that may evolve locally to nearly monomineralic löllingite ores (Hajjar et al., 2021). It also needs to be mentioned that gold and silver are highly concentrated in some ore zones (Bouabdellah et al., 2016), and that a post-ore supergene stage comprising rare arsenides and arsenates is characterizing the upper parts of mineralized structures.

Information on the nature of ore-forming fluids comes from a few fluid inclusion studies performed on the Bou Azzer ores (En-Naciri, 1995, Essarraj et al., 2005, Dolansky, 2007) and from some C, O and H isotopic data (Dolansky, 2007, Maacha et al., 2015). The obtained results are controversial. En-Naciri (1995) reported fluid inclusions of pre- and post-ore quartz and post-ore calcite containing moderate to highly saline fluids (15–22 wt% NaCl and 16.5–20.5 wt% $CaCl_2$) trapped at low temperatures (120–240 °C) under variable pressures (0.4–1.2 kb) in both pre-ore quartz and post-ore calcite. Essarraj et al. (2005) described a Co-Fe-As ore related with a late stage of Ag-Hg characterized by fluid inclusions with large halite crystals indicative of hyper-saline Na-Ca brines (16–24 wt% NaCl and 21–23 wt% $CaCl_2$) trapped at lower temperatures (120–200 °C) under a pressure range of 40–80 MPa. In contrast Dolansky (2007) found highly saline brines (31–42 wt% NaCl and 6–13 wt% $CaCl_2$) trapped at relatively high temperature (298–409 °C) under relatively high pressures (1.6–2.5 kb) in primary inclusions in pre-ore quartz. Dolansky (2007) also determined the salinity of secondary fluid inclusions (36–45 wt% NaCl and 13–26 wt% $CaCl_2$) in pre-ore quartz and of primary fluid inclusions in post-ore calcite (15.5–19.1 wt% NaCl and 20.9–21.5 wt% $CaCl_2$). She considered the high salinity, the homogenization temperature (164–290 °C) and trapping pressure (0.88–1.4 kb) of the former as representative of the ore-forming fluids. The lower salinity, temperature (≥200 °C) and pressure (~0.65 kb) of the inclusions in post-ore calcite indicate decreasing P-T trapping conditions over the course of mineral deposition. Maacha et al. (2015) and Dolansky (2007) also measured $\delta^{18}O$ and δD in quartz separates and a chlorite sample obtaining values of the precipitating fluids ranging from 7.9 to 9.6‰ $\delta^{18}O$ and from −62 to −30‰ δD with little variations among samples or deposits. These data were interpreted as signatures of magmatic water, whereas Maacha et al. (2015), on the basis of $\delta^{13}C$ (from −1.61 to −6.5‰) and $\delta^{18}O_{fluid}$ values (from −6.3 to 5.9‰) values in Bou Azzer calcite and dolomite, argued for the presence of exogenic water in the formation of the associated arsenide ore.

Published sulfur isotope data are scarce (Dolansky, 2007, Maacha et al., 2015) and hardly representative for the main ore-forming event as they provide a set of scattered $\delta^{34}S$ data from –32.3 to 9.9‰ obtained from galena, pyrite and chalcopyrite pertaining to the late epithermal stage.

Crosscutting and offsetting relationships led Leblanc and Billaud (1982) to conclude that all the orebodies postdate the serpentinization and the structures of the major Pan-African tectonic phase during which ophiolite obduction and greenschist metamorphism took place (685 ± 15 Ma; Rb/Sr, Clauer, 1976; 660-640 Ma, Blein et al., 2014). Leblanc and Billaud (1982) also observed that the main orebodies are located along transcurrent sinistral faults belonging to the ultimate Pan-African phase, between 615 and 580 Ma ago. Therefore, they did not rule out that this time relate to mineralization events in the district. Bouabdellah et al. (2016) argued that the Bou Azzer mineralization is younger than

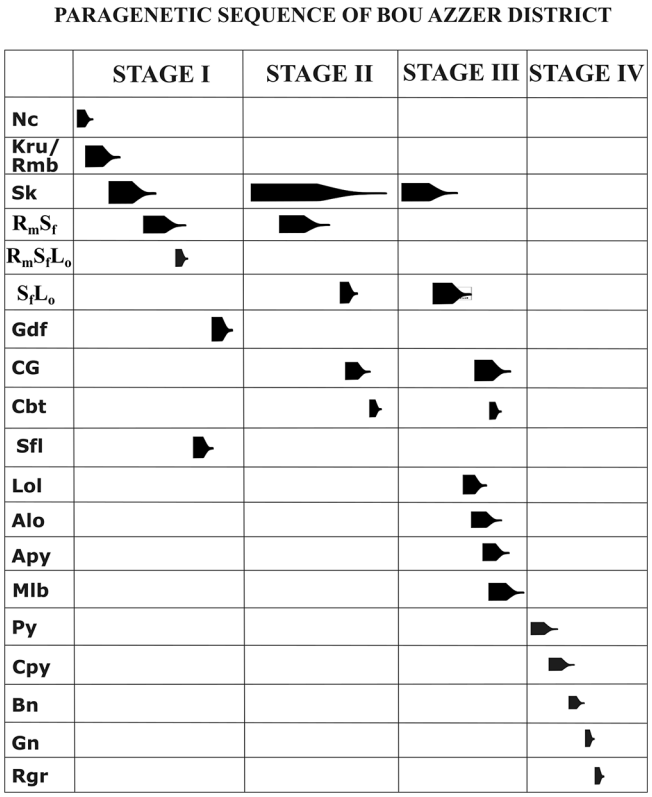

Fig. 2. Paragenetic sequence of arsenide ores from Bou Azzer district. Nc: nickeline, Kru/Rmb: krutovite/rammelsbergite, Sk: skutterudite, R_mS_f: crystals of rammelsbergite-safflorite solid solution, $R_mS_fL_o$: crystals of rammelsbergite-safflorite-Löllingite solid solution, S_fL_o: crystals of safflorite-löllingite solid solution, Gdf: gersdorffite, CG: crystals of cobaltite-gersdorffite solid solution, Cbt: cobaltite, Sfl: safflorite, Lol: löllingite, Alo: alloclasite, Apy: arsenopyrite, Mlb: molybdenite, Py: pyrite, Cpy: chalcopyrite, Bn: bornite, Gn: galena, Rgr: realgar.

the emplacement of the trachytic sills dated at 531 ± 5 Ma (U–Pb SIMS zircon ages) by Gasquet et al. (2005). A number of other radiometric studies aimed to date mineralization have yielded highly variable ages, from about 400 Ma down to 32 Ma, and their significance will be further discussed below. To sum up, a complex, telescoped and polymetallic (Co–Ni–As–Fe–Cu–Au–Ag) mineral district appears to be the result of late Pan-African and Variscan deformations and recrystallizations.

3. Sampling and analytical techniques

Specimens for microscopy and isotope investigations have been gathered from 5 Co-Ni deposits in the Bou Azzer area (Table 2). In particular, the study has mainly focused on three deposits (Fig. 3A-C); Tamdrost, Aghbar and Aït-Ahmane which are shortly described below as well as two other deposits (Filon 7/5 and Ightem) from which several samples were analysed for S isotopes. In addition, an examination of polished sections from Mechoui, Ambed and Agoudal added further support to the view that ores of the Bou Azzer district share a number of common features, such as a structural control and variable ore settings. Representative ore textures from some selected ores are shown in Fig. 4.

According to Maacha et al. (2015) the Tamdrost type ore bodies located at the discordant contact of serpentinites with felsic volcanic rocks of the Ouarzazate group are represented by veins and lenses filling fractures of extension and compression. A supergene alteration zone in serpentinite is the main ore-bearing structure hosting orebodies with maximum thickness at the contact of altered serpentinite.

Maacha et al. (2015) also show that the altered serpentinite is hosting ore veins at Aghbar that are related to synchronous fracturing and the ore body is restricted to the flanks of a serpentinite dome structure, whereas Dolansky (2007) pointed out that the mineralized structure at Aghbar is a broadly sub horizontal contact orebody with a concave-down form draped over the serpentinite massif. The structure is commonly described as a complex shell, owing to numerous subvertical lenses referred to as flamelike structures, attributed to the Hercynian deformations (Leblanc, 1975).

Aït-Ahmane does not refer to a single deposit but to an area in the easternmost part of the district where several ore veins are/were mined. The mineralization at Aït-Ahmane has been described as a "contact mineralization" that is hosted by lenses of calcified serpentinite located at the contact between serpentinite and quartz diorite or gabbro (En-Naciri, 1995) and as massive to disseminated bodies fully hosted by serpentinite (Hajjar et al., 2021). The former ore, taking the shape of disseminated, minute spherical aggregates, occurs essentially as an infilling in dissolution cavities within a mixture of clastic and chemical sediments. The latter ore fills intraserpentinite faults extending outwards through the fault walls filling small entwined veins and partly replacing serpentinite (Hajjar et al., 2021). These authors pointed out that serpentinite-hosted ores are atypical in that they are mainly formed by Fe diarsenides (löllingite) with very low Ni and Co contents. Mineral textures show that ore-forming fluids partly have dissolved serpentine and, subsequently, precipitated Fe-rich arsenide ores.

Various types of samples have been analysed for their (Pb, Sr, Nd and S) isotopic and geochemical signatures. The fine-grained nature of the ores poses a challenge during the stage of sample selection for (S and Pb) isotope analyses. The di-, tri-arsenide and sulfarsenide minerals from different depositional stages, and encompassing all morphological types, were selectively sampled from polished sections by using a rotatory tool (DremelTM) equipped with LascoTM 1.58 mm and 2.38 mm diamond core drills. As a complement, a few course Bou Azzer ore samples were also taken from the mineral collection of the Swedish Museum of Natural History. These specimens allowed separation of enough material for doing Sr-Nd isotope work, but their exact locality is not known. Regional rocks were selected to encompass plausible source rocks of mineralizing components at the time of ~~o~~re formation.

Before the Sr-Nd-Pb-isotope ratio measurements, minerals and whole rock samples were spiked with a mixed $^{147}Sm/^{150}Nd$ spike solution (a mixed ^{84}Sr-^{87}Rb spike was also added to museum ore samples aimed for Rb-Sr analysis) and digested in nitric acid and a HF-$HClO_4$ acid mixture, respectively. Initially, dissolved samples went through an ion exchange column set-up using a mixture of TrueSpec® of AG1x8 resins. Sr was further purified in a second pass through the same columns now filled with SrSpec® resin, whereas Nd (and Sm) was isolated in Ln-spec columns (Pin and Zalduegui, 1997). The Pb fractions were re-dissolved in HBr, and treated further in columns with AG1 × 8, Cl^- form resin.

A Thermo-Finnigan Triton thermal ionization mass spectrometry (TIMS) instrument was used for the Sr and Nd isotope analyses and data were normalized to $^{88}Sr/^{86}Sr = 0.1194$ and $^{146}Nd/^{144}Nd = 0.7219$, respectively. Additionally, replicate analyses of the NBS-987 Sr standard analyzed during the course of the study yielded an average $^{87}Sr/^{86}Sr = 0.710221 \pm 0.000011$ (2σ external precision). Corresponding analyses of the La Jolla Nd standard yielded an average $^{143}Nd/^{144}Nd = 0.511848 \pm 0.000009$ (2σ external precision). Estimated external uncertainties amount to ca. ± 0.4 and ± 0.00005 for the calculated εNd and Sr initial isotope values, respectively. Pb isotope analyses were performed with a Nu Plasma II ICP-MS instrument (hosted by the Vegacenter facility), with Tl added to allow for an internal correction of the mass bias, and the measured intensities were corrected for background and Hg interference on mass 204. The NBS-981 Pb standard was run at regular intervals and all unknowns were analyzed in duplicate. The obtained values for the standard are within error of those given by Todt et al. (1996), and the external reproducibility is between 0.04% ($^{206}Pb/^{204}Pb$) and 0.08% ($^{208}Pb/^{204}Pb$).

Sulfur isotope analyses were performed at the Laboratorio de Isótopos Estables (University of Salamanca, Spain). Sulfur isotopic ratios

Table 2
Co-Ni-Fe ore samples age according to the geochronologic dating of the ore deposit Sample Localization Age Ma/Reference.

Sample	Localization	Age Ma / Reference
		Paleozoic
759 972 1281 2456 2457	Filon 7/5 Filon 7/5 Filon 7/5 Filon 7/5 Filon 7/5	Brannerite associated to skutterudite (383 ± 7 Ma to 355 ± 10 Ma, U/Pb, (Dolansky, 2007)); Brannerite associated to altered skutterudite, chlorite and molibdenite (257 ± 8 Ma to 32 ± 2 Ma, U/Pb, (Dolansky, 2007)); Adularia associated to sulfide (215 ± 8 Ma, Ar-Ar, (Leveresse, 2001); Molybdenite-rich sulfides (350 Ma – 371 Ma, Re-Os, (Oberthür et al., 2009)); Carbonates and brannerite coexisting with molibdenite (308 ± 31 Ma, Sm-Nd (Oberthür et al., 2009))
728 727 726 819 1026 722 819 722 543 724 689 824 670a 805a3 843	Aghbar Aghbar Aghbar Aghbar Aghbar Aghbar Aghbar Aghbar Aghbar Aghbar Aghbar Aghbar Aghbar Aghbar Aghbar	Molybdenite-rich sulfides (400 ± 2.5 Ma, Re-Os, (Oberthür et al., 2009)
2101 1551 1643 542	Tamdrost Tamdrost Tamdrost Tamdrost	Muscovite present from Early stage to sulfide stage (392 ± 15 Ma; 356 ± 20 Ma, Ar-Ar (Leveresse, 2001)
79	Ightem	
2418 2445 999	Aït-Ahmane Aït-Ahmane Aït-Ahmane	Carbonates and brannerite coexisting with molibdenite (308 ± 31 Ma, Sm-Nd, 310 ± 5 Ma, U/Pb, (Oberthür et al., 2009))

of arsenide and sulfarsenide minerals were obtained by pyrolysis on an Elemental Analyzer (Eurovector EA3000) coupled on line with an Isoprime (Micromass) continuous flow mass spectrometer. The SO_2 liberated by standard stable isotopic extraction techniques (Coleman and Moore, 1978) was analyzed using a dedicated SITA-II (VGIsogas) dual inlet mass spectrometer. Due to the small SO_2 quantities produced in both methods, V_2O_5 was added to favour combustion.

Sulfur from regional rocks was separated using a chemical extraction technique based on the works of Canfield et al. (1986) and Hall et al. (1988), with modifications as described by Recio et al. (1991). Results are reported in the standard delta per mil notation relative to Canyon Diablo Troilite (CDT). Replicate analysis of reference standards gave an average reproducibility of ± 0.3‰.

Element concentrations of whole rock samples were determined at Intertek Laboratories (Australia). Sample preparation was performed by four acid digestion offering a near total dissolution of all mineral species. All elements were analyzed by combined ICP-OES and ICP-MS methods for ultra-trace levels under the control of certified international standards. Further details on the latter, as well as calibration, detection limits, etc., can be found at http://www.intertek.com/minerals.

4. Results

Ore samples were analyzed mainly for their lead and sulfur isotope composition, and for a few of these also Sr and Nd isotope analyses were carried out. Further, to establish the source of metals in nearby Bou Azzer ores, radiogenic (Pb-Sr-Nd) isotope data, along with some S isotope analyses and geochemical results, have been acquired from a suite of potential source rocks. Most of the sampled rocks are Neoproterozoic, comprising either a Cryogenian ophiolitic suite or are sedimentary, volcano-sedimentary and granitic rocks of a similar age (Table 1). Others formed during the Ediacaran period.

4.1. Pb isotopes:

The results of Pb-isotope analysis of twenty-four ore samples and nineteen regional rock samples are given in Tables 3 and 4 and presented on conventional Pb-isotope diagrams in Figs. 5 and 6. $^{206}Pb/^{204}Pb$, $^{207}Pb/^{204}Pb$ and $^{208}Pb/^{204}Pb$ ratios of the arsenide and sulfide ores cover a wide range between 15.79 and 56.93, 15.13–17.71 and 34.85–38.66, respectively. One löllingite sample (#1643/10) from Tamdrost has a remarkably unradiogenic composition ($^{206}Pb/^{204}Pb$ = 15.79), and an arsenopyrite sample (#819) from Aghbar has also a deviating, unradiogenic composition ($^{206}Pb/^{204}Pb$ = 16.71). Another outstanding feature is that a significant number of ore samples from the Aghbar and Tamdrost deposits are strongly radiogenic and tend to define linear uranogenic trends with relatively flat slopes (Fig. 5A, inset). Other ore samples display a relatively limited data variation with

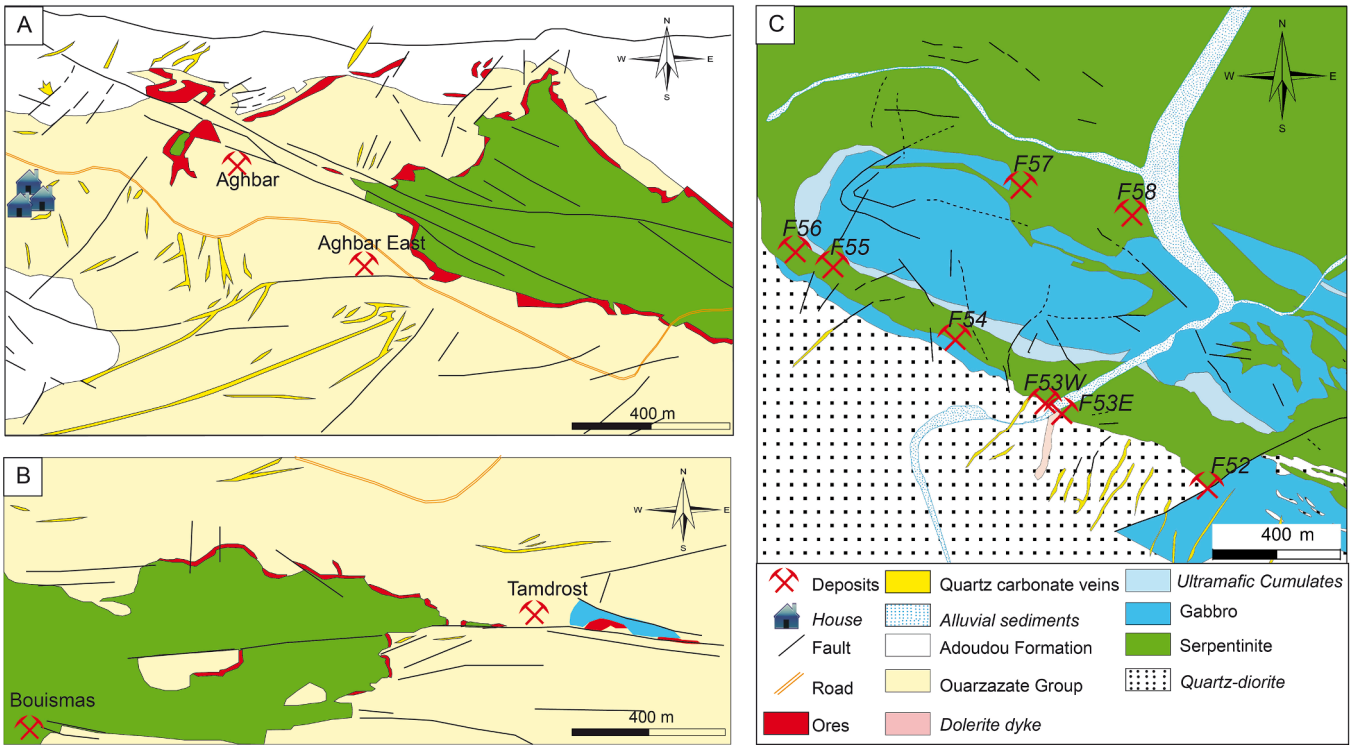

Fig. 3. (A) Geological map of Aghbar deposit (modified after Leblanc, 1981). (B) Geological map of Tamdrost deposit (modified after Leblanc, 1981). (c) Geological map of Aït-Ahmane area (modified from Saquaque et al., 1992), showing the location of the differente ore deposits.

e.g. $^{206}Pb/^{204}Pb$ between ca 17.9 and 18.1, but since this group of samples show a significant range in their $^{207}Pb/^{204}Pb$ ratios for a given $^{206}Pb/^{204}Pb$ ratio it becomes somewhat ambiguous to tell exactly which samples define the flat trends. Yet, if such trends are interpreted as isochrones originating from an approximative bulk ore signature, and by excluding two Tamdrost (1643/34 and 1643/10) and three of the Aghbar samples (724, 819 löll and 1026) plotting below reasonable arrays, their slopes suggest ages at 392 ± 48 Ma (MSWD = 3.2) and 400 ± 150 Ma (MSWD = 30) for Aghbar (n = 10 samples) and Tamdrost (n = 6), respectively. A combined regression involving Aghbar and Tamdrost samples yields an age of 382 ± 52 (MSWD = 12). Although there is a clear variation in $^{207}Pb/^{204}Pb$ data from the Aït-Ahmane deposit ($^{206}Pb/^{204}Pb$ close to 18.0) that exceeds the analytical precision, the compositional range is narrower compared to the other deposits, although this could be the result of the restricted number of samples collected from this deposit (Table 3). The thorogenic lead systematics of ore minerals (Fig. 5B) seem also quite complex given that a range of specimens have significantly radiogenic, and variable, $^{206}Pb/^{204}Pb$ in combination with comparatively low $^{208}Pb/^{204}Pb$, in consistency with very low apparent Th/U ratios of these minerals. The remaining ore minerals cluster in a comparatively unradiogenic region and tend to form a crude linear, steep array.

Rocks of the ophiolite suite (e.g. gabbro and serpentinite) and associated rocks (e.g. Qz-diorite and rodingite) have relatively unradiogenic compositions with $^{206}Pb/^{204}Pb$ between ca. 18.0 and 18.4 (Table 4) that are similar to, or slightly more radiogenic, than the bulk of ore data. However, in analogy with the situation for some ore specimens, data for certain rock samples span a large Pb isotope interval (Fig. 6). The extreme values are defined by an unradiogenic composition of a pegmatite (T-pegm; $^{206}Pb/^{204}Pb$ = 15.49) and radiogenic data for a dolomite (WB-Dol; $^{206}Pb/^{204}Pb$ = 37.25), respectively. There is no systematic isotope pattern to be seen if the inferred stratigraphic ages for different rocks are taken into account; yet, e.g. the composition of the T-peg sample would argue for an Early Proterozoic time of emplacement. Tentatively, certain rock data form crude linear arrays in the uranogenic diagram (Fig. 6A), but their significance is not obvious as further discussed below. With regard to the thorogenic lead, rock data tend to develop an array defining a steep slope (stippled line in Fig. 6B) and the bulk ore composition plots close to this array whose end-members are defined by basement rocks. As also noted for the ore minerals, there is a tendency for a few rocks to show high $^{206}Pb/^{204}Pb$ ratios but without correspondingly elevated $^{208}Pb/^{204}Pb$ values.

4.2. Sr isotopes:

Only a few Rb-Sr analyses were carried out on museum ore specimens; two skutterudite, one erythrite and one carbonate. The obtained $^{87}Sr/^{86}Sr$ values are quite homogeneous and close to 0.710 (Table 5). The calculation of their initial Sr isotope values is not obvious to carry out since the age of mineralization is still a debated issue. However, the obtained Rb/Sr ratios are generally low implying that the back-calculation to a desired time(s) of ore formation is not critically dependent on the exact age. By using an average ore mineralization age of 350 Ma (see discussion below), the calculated initial values of ore minerals fall between 0.709 and 0.710 (Table 5). A first order approximation suggests these values to be a good estimate of the strontium isotope signature carried by Bou Azzer ore-forming solutions.

Rock data, on the other hand, are more heterogeneous which is an expected feature given that the data set involves rocks of different ages and origin and data scatter a lot in a conventional Rb-Sr isochron diagram (not shown). Partly, the scatter may be due to possible disturbances of the Rb-Sr system which in turn would affect calculated initial Sr isotope compositions. Such compositions, calculated using the inferred emplacement ages tabulated in Table 5, are between 0.7019 and 0.7060 for the dolomite, the rhyolite, a Qz-diorite and three rocks (serpentinite, dunite and gabbro) believed to belong to the ophiolite suite. No Sr concentration data is available for the analyzed clinopyroxenite (OPH-cpx3); however, its Rb concentration is low (0.29 ppm) and knowing that clinopyroxene is usually a Ca-rich phase (by inference also with an elevated Sr content) it is suggested that the initial Sr isotope

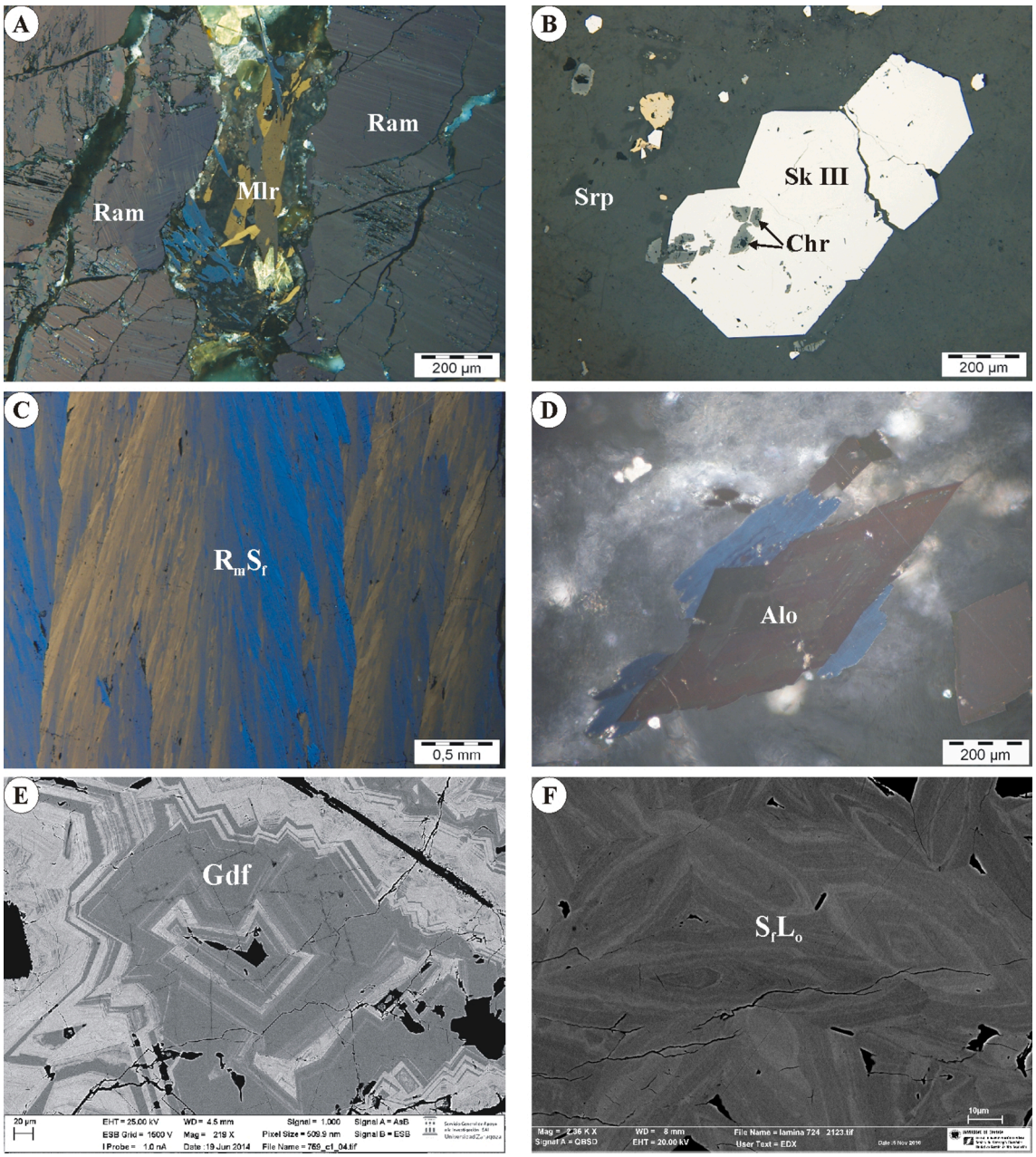

Fig. 4. Reflected-light photomicrographs (A-D) and Back Scattered electron images (E-F) showing representative mineralogy of the studied ore deposits from Bou Azzer arsenide ores (Morocco). (A) Massive rammelsbergite exhibiting anisotropic colors with lamellae and inversion-induced polysynthetic twins; the crack in the middle of the masse is filled by millerite; #670a, Aghbar. (B) Euhedral crystals of skutterudite III, including small chromian spinel grains, scattered in serpentinite; #728, Aghbar. (C) Rammelsgergite-Safflorite solid-solution crystals with plumose textures; #1643–3, Tamdrost. (D) Idiomorphic crystals of alloclasite; #2449 Aït-Ahmane. (E) Crystals of arsenian- gersdorffite showing oscillatory replacement-induced zoning, very fine in scale along crystallographic directions; #759a, Filon7/5. (F) Rhythmic compositional zoning in löllingite–safflorite solid-solution crystals; #724, Aghbar. Abbreviations: Ram: rammelsbergite; Mlr: millerite; Sk III: skutterudite from stage III; Chr: chromian spinel; Srp: serpentinite; R_mS_f: rammelsbergite-safflorite solid-solution series; Alo: alloclasite; Gdf: gersdorffite; S_fL_o: safflorite-löllingite solid-solution series.

composition is close to the measured value of 0.7107. Knowing that the Rb-Sr system is susceptible to isotopic disturbances induced by metamorphic and hydrothermal processes one should treat initial values, whether calculated for an emplacement age or a mineralization age, with caution. This uncertainty is further accentuated by the question mark regarding the emplacement ages of some rocks (see discussion) and also by the calculated initial value of ca. 0.7025 for the analyzed carbonate rock of the ~ 789 Ma Tachdamt-Bleida group which is well below that of contemporaneous seawater (0.7068, Asmerom et al., 1991). Probably, this reactive type of sample has also suffered some kind of disturbance, or carries minute inclusions of potassium-rich clay minerals, which is supported by its unusually high $^{87}Rb/^{86}Sr$ ratio of 0.656.

4.3. Nd isotopes:

The analyses of five ore samples (two carbonates, two skutterudites and one erythrite) yielded highly variable results (Table 6). The spiking procedure turned out to be a major problem and the reason is probably the presence of variable amounts of REE-rich inclusions, such as brannerite, in the analyzed minerals which led to both over- and underspiked sample mixtures. Therefore, ore mineral results must be treated with

Table 3
Pb isotope compositions of ore minerals from selected Co-Ni arsenide ores in the Bou Azzer area.

Sample	Mineral	Deposit	$^{206}Pb/^{204}Pb$	2σ	$^{207}Pb/^{204}Pb$	2σ	$^{208}Pb/^{204}Pb$	2σ
1026	Skutterudite	Aghbar	17.978	0.011	15.371	0.011	36.177	0.035
726	Arsenopyrite	Aghbar	32.989	0.011	16.396	0.011	38.599	0.035
819	Arsenopyrite	Aghbar	16.706	0.011	15.481	0.011	36.399	0.035
805a3	Arsenopyrite	Aghbar	53.511	0.025	17.477	0.006	37.694	0.018
724	Löllingite	Aghbar	19.792	0.011	15.477	0.011	35.974	0.035
543	Löllingite	Aghbar	19.354	0.011	15.609	0.011	38.376	0.035
722	Skutterudite	Aghbar	18.588	0.020	15.583	0.015	37.903	0.046
728	Skutterudite	Aghbar	19.485	0.016	15.630	0.011	37.920	0.035
843	Skutterudite	Aghbar	18.061	0.019	15.544	0.015	37.855	0.048
670a	Rammelsbergite	Aghbar	23.664	0.011	15.857	0.011	38.589	0.035
670a	Nickeline	Aghbar	22.664	0.037	15.829	0.015	38.664	0.035
728	Rammelsbergite	Aghbar	18.916	0.027	15.616	0.011	37.406	0.035
819	Löllingite	Aghbar	16.706	0.011	15.496	0.011	36.392	0.035
1643/34	Skutterudite	Tamdrost	17.606	0.011	15.288	0.011	35.431	0.035
1643/24	Skutterudite	Tamdrost	48.074	0.005	17.096	0.006	38.186	0.018
2101	Skutterudite	Tamdrost	35.090	0.011	16.485	0.011	37.463	0.035
1643/10	Löllingite	Tamdrost	15.789	0.011	15.132	0.011	34.855	0.035
1643/24b	Skutterudite	Tamdrost	56.925	0.011	17.706	0.011	38.231	0.035
1643–3	Skutterudite	Tamdrost	31.380	0.046	16.246	0.013	37.537	0.038
1551	Löllingite	Tamdrost	17.924	0.011	15.524	0.011	37.703	0.035
1643–4	Rammelsbergite	Tamdrost	18.729	0.011	15.580	0.011	37.789	0.035
999a	Löllingite	Ait-Ahmane	18.045	0.011	15.636	0.011	37.996	0.035
999b	Löllingite	Ait-Ahmane	18.078	0.016	15.558	0.011	38.003	0.035
2415	Löllingite	Ait-Ahmane	18.039	0.011	15.533	0.011	37.964	0.035

Table 4
Pb isotope compositions of selected country rocks from the Bou Azzer area.

AgE-1	Andesitic tuffs	Ediacaran	29.341	0.013	16.149	0.011	43.91	0.035	22.393	15.778	15.959	15.326
Tiddiline	Sandstone	Ediacaran	18.548	0.011	15.999	0.011	38.264	0.035	18.124	15.536	17.73	15.509
WBW2	Granodiorite	Ediacaran	25.276	0.005	15.999	0.011	41.159	0.035	21.392	15.791	17.795	15.539
Q Diorite	Quarzt-diorite	Upper Cryogenian	18.679	0.017	15.572	0.011	38.042	0.026	18.398	15.557	15.859	15.326
Q Di-6	Quarzt-diorite	Upper Cryogenian	18.629	0.011	15.59	0.011	38.326	0.035	18.347	15.557	18.086	15.557
Rodingite	Rodingite	Upper Cryogenian	18.423	0.011	15.57	0.011	38.304	0.035	18.188	15.558	18.416	15.57
B1, serp.	Serpentinite	Upper Cryogenian	17.866	0.011	15.523	0.011	37.666	0.035	17.862	15.522	17.86	15.522
cpx, cumulates	Clinopyroxenite	Upper Cryogenian	19.161	0.058	15.652	0.006	37.885	0.026	18.946	15.641	18.747	15.627
OPH-cpx3	Clinopyroxenite	Upper Cryogenian	20.636	0.018	15.731	0.011	40.868	0.035	20.425	15.719	20.229	15.705
OPH-DUN 4	Dunite	Upper Cryogenian	18.186	0.011	15.586	0.011	37.87	0.035	17.654	15.558	17.162	15.523
OPH-CR1	Chromitite	Upper Cryogenian	18.278	0.011	15.588	0.011	37.881	0.035	18.268	15.587	18.258	15.587
OPH-Ga2	Gabbro	Upper Cryogenian	18.395	0.011	15.569	0.011	38.23	0.035	18.093	15.552	17.813	15.533
T Pegm	Pegmatite	Lower Cryogenian	15.488	0.005	15.233	0.007	34.987	0.018	15.44	15.231	15.396	115.227
T ORGN	Orthogneiss	Lower Cryogenian	27.61	0.011	16.545	0.011	46.499	0.051	24.948	16.384	21.813	16.189
TAK-2a	Rhyolite	Lower Cryogenian	19.036	0.011	15.582	0.011	37.956	0.035	18.326	15.544	17.669	15.497
Trh 40	Rhyolite	Lower Cryogenian	25.849	0.011	16.02	0.011	46.002	0.051	21.611	15.794	17.686	15.518
BW-3	Volcanosediments	Lower Cryogenian	18.958	0.005	15.693	0.006	38.886	0.018	18.44	15.665	17.959	15.632
FW-3	Volcanosediments	Lower Cryogenian	19.06	0.013	15.639	0.011	38.969	0.035	18.54	15.611	18.058	15.577
DOL WB	Dolomite	Lower Cryogenian	37.251	0.011	17.597	0.006	39.211	0.018	35.662	17.512	34.19	17.409

caution and the calculated span of ƐNd (ore, 350 Ma) values between −6.5 and 11 is highly uncertain. The analyses of rocks involved eleven samples and obtained Nd isotope compositions and calculated parameter values are shown in Table 6 and displayed on Fig. 7. ƐNd values were calculated both for an inferred emplacement age (using ages in Table 1) and an ore event at 350 Ma. ƐNd (658 Ma) values for rocks of the ophiolite suite, except for the serpentinite (B1 serp) yielding a negative value, have values between 3.06 and 5.05 that are similar, or slightly lower, than published data of similar rocks (D'Lemos et al., 2006). Also, an andesitic tuff (Age-1), and a quartz-diorite (Qz-Di6) have similar values, whereas data for other rocks (pegmatite, volcanic sediment, rhyolite, orthogneiss and carbonate) have more variable and negative values. At the time of the inferred 350 Ma ore-forming event, negative ƐNd values characterize most rocks except for the quartz-diorite, the andesitic tuff (Age-1) and the ophiolitic rock types (except B1 serp.).

4.4. S isotopes:

The S isotope study includes in-situ analyses of ore stage samples from Filon 7/5 and Ightem in addition to samples from those three deposits (Aghbar, Tamdrost and Aït-Ahmane) for which Pb isotope data exist (Table 7). The results are the first-ever S isotope analysis obtained from minor amounts of sulfur contained in arsenides and sulfarsenides. The set of analyzed samples covers the three sub-stages in which the main Co–, Ni-, Fe-rich arsenide and sulfarsenide stage (stage II; Bouabdellah et al., 2016) can be subdivided: Ni-Co dominant (IIa), Co-Fe dominant (IIb) and Fe-Co dominant (IIc). The heterogeneous impression yielded by the relatively few published S isotope data obtained from the post-ore, epithermal stage (a $\delta^{34}S$ range from + 10 to –32 ‰; Maacha et al., 2015, Dolansky, 2007) is reinforced by the new data from the main ore-forming stage. The entire $\delta^{34}S$ data range defined by thirty-six stage II specimens is from + 11.2 to –22.5 ‰, with no easily discernible distinction between data representing different ores and different sub-stages (Fig. 8). For instance, there is a large data spread characterizing both Filon 7/5 and Aghbar (the range in both cases is more than 22 ‰, involving both negative and positive values), with a mode fairly close to zero per mille. Aït-Ahmane samples also display a large spread in data, but all numbers are negative, whereas Tamdrost and Ightem (few data) have values clustering around zero. Whenever related data exist from

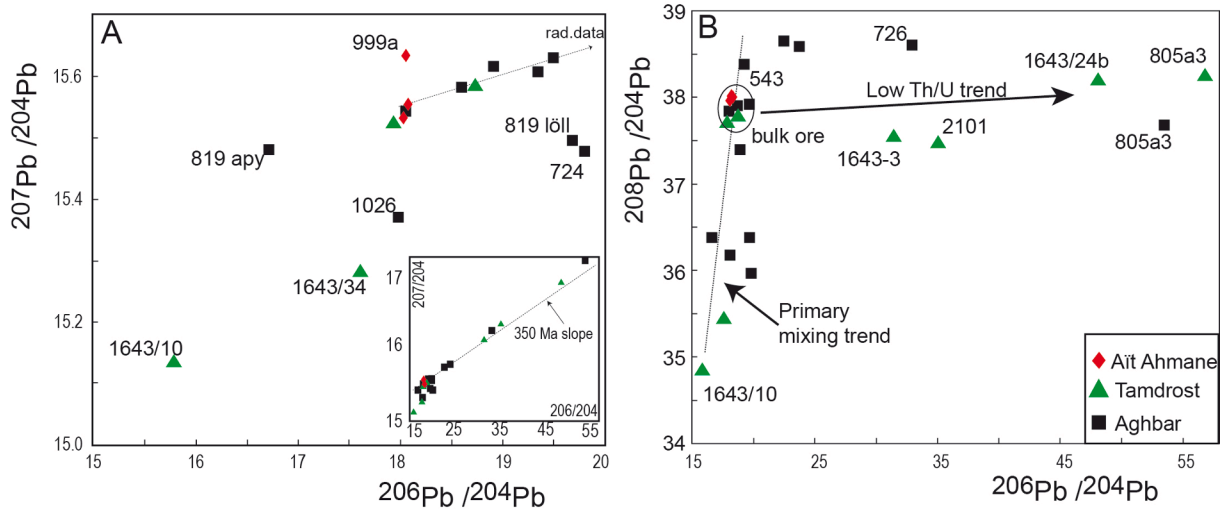

Fig. 5. Lead isotopic compositions of ore phases from three deposits in the Bou Azzer area. A) a $^{207}Pb/^{204}Pb$ versus $^{206}Pb/^{204}Pb$ plot. The inset shows the full range of obtained compositions. Added is a reference line with a slope corresponding to the preferred ore formation age (350 Ma); B) a $^{208}Pb/^{204}Pb$ versus $^{206}Pb/^{204}Pb$ plot. The hatched line is likely depicting a potential *syn*-ore mixing effect, whereas the flat line illustrates the effect of an in-situ effect controlled by U-rich and Th-poor inclusions.

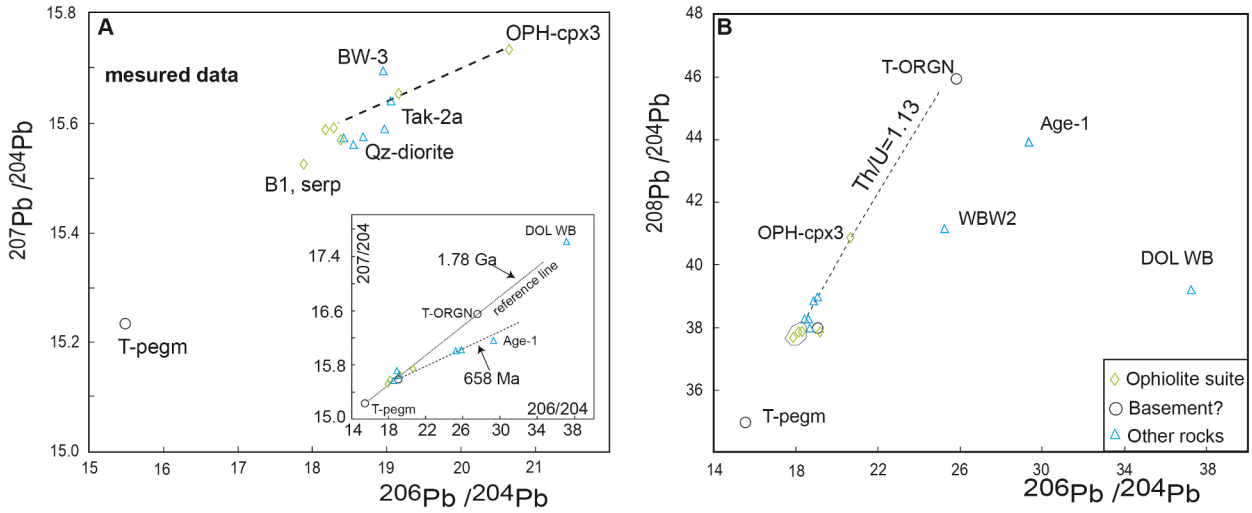

Fig. 6. Lead isotopic compositions of selected whole rocks, occurring at distal positions from known ore occurrences, in the Bou Azzer area. The encircled areas in diagrams approximate the isotopic signature of the ophiolite magma ($^{206}Pb/^{204}Pb = 18$, $^{207}Pb/^{204}Pb = 15.6$ and $^{208}Pb/^{204}Pb = 38$), and this composition is also used as a starting point of a line connecting samples with an ophiolitic chemistry. A) a $^{207}Pb/^{204}Pb$ versus $^{206}Pb/^{204}Pb$ plot. The steep dotted line in the inset aligns three samples (T-pegm, Tak-2a and T-ORGN) that might exemplify isolated remnants of a Proterozoic basement, whereas the hatched line in the main diagram is drawn to connect rocks with an ophiolitic chemistry; B) a $^{208}Pb/^{204}Pb$ versus $^{206}Pb/^{204}Pb$ plot.

two nearby spots hitting the same mineral (e.g. 759a and 759b gersdorffite in Table 7), a relatively minor isotopic difference is noted although it often exceeds the analytical precision.

Five analyses correspond to whole rocks representing the ophiolite suite. Apart from one negative value (-2.2‰ for a gabbro), the remaining values are clearly positive defining a range between 6.2 and 9.0 ‰.

4.5. Geochemistry of rocks

Nineteen rocks were analyzed for major and trace elements. The purpose of this work that involves fifthteen rock types taken from outcrops in the vicinity of ore deposits (see Tables 8(A-C); Fig. 1) was basically to provide basic information about samples also used for isotope analyses. In the current context, it is crucial that selected samples were not affected by post-emplacement ore-bearing fluids in order to enable a meaningful interpretation of isotope data of rocks and their possible role as sources of ore elements. For instance, although the Co contents in two samples also used for isotope work (B1, serpentinite; 197 ppm and OPH-Dun4 dunite; 130 ppm) are much higher than in remaining samples (Table 8B), these numbers are not especially high in comparison with average Co concentrations in ultramafic rocks in general (110 ppm; Stueber and Goles, 1967) and with previous ophiolite data from Bou Azzer (Hajjar et al., 2021). Hence, there is little evidence to suggest that samples used for isotope work have suffered an isotopic over-printing effect in relation to the ore-forming event(s). However, it is less certain that e.g. the Rb-Sr isotope whole-rock system has stayed closed ever since the time of rock crystallization given that e.g. volcanic rocks of the ophiolite suite were affected by regional metamorphism, obduction-related metamorphism and basalt-seawater interaction (Naidoo et al., 1991). Geochemical Rb, Sr, U, Th and Pb concentrations were also used for calculating initial Sr and Pb isotope compositions both at the inferred time of rock emplacement and that of ore formation.

Table 5
Rb-Sr isotope data of selected rocks and ore specimens from the Bou Azzer area.

	Lithology	Rb	Sr	$^{87}Sr/^{86}Sr$,mean	2 sigma	$^{87}Rb/^{86}Sr$	Rock age	$^{87}Sr/^{86}Sr$,i(rock)	$^{87}Sr/^{86}Sr$,i(ore)
whole rockOPH-cpx3	clinopyroxenite	0.29	no data	0.710715	27	≤0.1	658	0.71070	0.7107
Age-1	andesitic tuff	114.7	19.58	0.793744	8	17.087	567	0.65561	0.70861
BW-3	volc. sediment	99.82	40.29	0.790322	9	7.226	767	0.71115	0.75432
Tak-2a	rhyolite	41.9	208.16	0.708510	6	0.582	767	0.70211	0.70561
DOL WB	dolomite	8.24	36.36	0.709938	10	0.656	789	0.70255	0.70667
Q-Di6	Qz-diorite	8.52	235.1	0.704365	8	0.105	650	0.70339	0.70384
B1 serp	serpentinite	4.02	4.47	0.726406	14	2.607	658	0.70194	0.71342
OPH-Dun4	dunite	2.03	14.81	0.709713	7	0.397	658	0.70599	0.70774
OPH-Ga2	gabbro	20.26	510.6	0.704392	6	0.115	697	0.70325	0.70382
T pegm	pegmatite	201.4	217.7	0.781318	8	2.696	700	0.75439	0.76789
T-ORGN	orthogneiss	266.8	46.8	1.029491	5	17.013	754	0.84635	0.94472
mineralM1 erytrit		0.10	548	0.710198		less than0.001			0.71020
M2 skutterudit		1.90	53	0.709459		0.102			0.70895
M3 carbonat		0.14	161	0.709192		0.003			0.70918
M3 skutterudit		0.05	36	0.710203		0.004			0.71018

Table 6
Sm-Nd data for selected rocks and ore specimens from the Bou Azzer area.

whole rock										
OPH-cpx3	clinopyroxenite	2.81	8.76	0.512861	6	0.1941	1.92	658	4.6	4.5
Age-1	andesitic tuff	2.85	18.19	0.512472	6	0.0947	0.79	567	4.2	1.3
BW-3	volc. sediment	6.27	32.48	0.511760	d:0	0.1166	2.11	767	−9.3	−13.6
Tak-2a	rhyolite	0.44	1.58	0.512395	d:0	0.1690	2.45	767	−2.0	−3.5
Tak-2a aug20	duplicate	0.44	1.65	0.512359	6	0.1603	2.14	767	−1.9	−3.8
DOL WB	dolomite	0.83	2.35	0.512518	7	0.2139	n.d.	789	−4.1	−3.1
Dol-WB aug20	duplicate	0.72	2.15	0.512496	4	0.2030	n.d.	789	−3.4	−3.8
Q-Di6	Qz-diorite	4.04	16.41	0.512707	5	0.1489	0.91	650	5.3	3.5
B1 serp	serpentinite	0.16	0.83	0.512281	10	0.1179	1.30	658	−0.4	−3.5
OPH-Dun4	dunite	0.03	0.13	0.512578	8	0.1401	1.07	658	3.6	1.4
OPH-Ga2	gabbro	2.61	10.54	0.512694	5	0.1497	0.95	658	5.1	3.2
T pegm	pegmatite	1.24	5.03	0.512050	d:0	0.1495	2.52	700	−7.3	−9.4
T-ORGN	orthogneiss	5.61	39.72	0.511824	d:0	0.0854	1.52	754	−5.2	−10.9
mineral										
M1 erythrite	3.27	6.14	0.512591	6	0.3224	n.d.	−6.5			
M2 skutterudite	0.14	3.24	0.512485	12	0.0258	0.49	4.7			
M2 carbonate	16.27	51.58	0.512773	3	0.1908	2.26	2.9			
M3 carbonate	5.07	47.94	0.512912	6	0.0640	0.17	11.3			
M3 skutterudite	4.46	3.00	0.512887	11	0.8986	n.d.	−26.6			

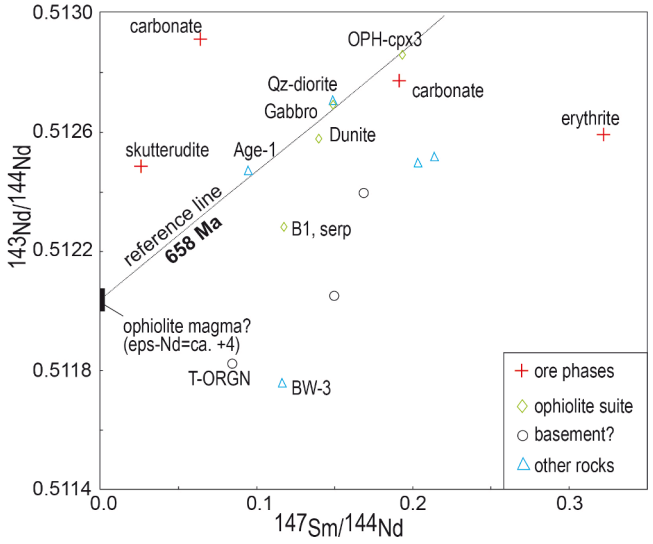

Fig. 7. A Sm-Nd isotope plot of selected whole rocks and ore minerals from the Bou Azzer area. Rocks of the ophiolite suite have a common age of ca. 658 Ma, and this age is also indicated by the slope of an added reference line that crudely connects some rocks of this suite.

5. Discussion

Published field, mineralogical, petrological, fluid inclusion and isotopic data indicate that ore depositional conditions have varied across the Bou Azzer district. Although our study is focused on only three, geographically spread out, ores (Tamdrost, Aghbar and Aït-Ahmane), these ores share features in different types of isotope (Pb, Sr and Nd) diagrams, as further discussed below. This is suggesting that elements in different deposits have a similar origin and that the conclusions drawn thus have a regional significance. The radiogenic isotope systematics are clearly complex for rocks and minerals analyzed from the sampled ores in this study; however, it is still possible to use isotopic, mineralogical and field information to constrain the sources of ore components, and to discuss the timing and general processes leading to ore formation. Two features are of outmost importance for controlling radiogenic (Pb, Nd and Sr) isotope systematics pertinent to ore-forming conditions; assimilation of probably both sedimentary cover rocks and basement rocks during Neoproterozoic magma formation and the common incorporation of (U- and REE-bearing) brannerite inclusions in arsenides and sulfarsenides, and related in-situ growth of radiogenic lead isotopes ever since ore mineral formation.

5.1. Lead isotope constraints on the ore-forming conditions

The lead isotope systematics of ore minerals and rocks show some unusual features involving e.g. highly evolved isotopic compositions and

Table 7
Sulfur isotope composition of ore minerals and country rocks Deposit Sample Stage Mineral δ ^{34}S.

F7/5	759a	St II a	Gersdorffite	9.6
	759b	St II a	Gersdorffite	11.2
	972a	St II a	Rammelsbergite-Löllingite	−11.1
	972b	St II a	Skutterudite	−0.1
	972b	St II a	Gersdorffite	7.5
	972c	St II a	Gersdorffite	1.4
	1281a	St II a	Skutterudite	5.4
	1281b	St II a	Skutterudite	5.3
	2456	St II a	Skutterudite-Rammelsbergite	2.2
	2457	St II a	Nickeline	7.7
Aghbar	728	St II a	Skutterudite I	−6.5
	727	St II a	Skutterudite I	4.9
	726	St II b	Skutterudite II	4.3
	819	St II b	Skutterudite II	6
	1026	St II b	Skutterudite II	3.8
	722	St II c	Arsenopyrite	6.3
	819	St II c	Löllingite	−16
	722	St II c	Arsenopyrite	1.3
	543	St II c	Löllingite	3
	724	St II c	Löllingite	5.6
Tamdrost	2101	St II a	Skutterudite I	1.7
	1551	St II a	Skutterudite I	3.6
	1643/3	St II b	Skutterudite I	2.3
	1643/3	St II b	Skutterudite II	−0.5
	1643/34	St II b	Skutterudite II	−0.1
	1643/24b	St II b	Rammelsbergite-pararammelsbergite	0.7
	1643/4	St II a	Löllingite	−1.8
Ait Ahmane	2418	St II a	Skutterudite I	−3.3
	2445	St II b	Skutterudite II	–22.5
	999a	St II c	Löllingite	−5.1
	999b	St II c	Löllingite	−3.7
	2415	St II c	Löllingite	−6.5
	999a	St II c	Arsenopyrite	−9.9
	2449	St II c	Alloclasite	−13.1
Ightem	79		Skutterudite	5.4
	79b		Skutterudite	4.7
Regional	Qdi-6		diorite	6.2
Rock	OPH-Dun4		ophiolite	7.5
	OPH-Ser		ophiolite	9
	OPH-Ga2		ophiolite	−2.2
	Rodingite		ophiolite	8.7

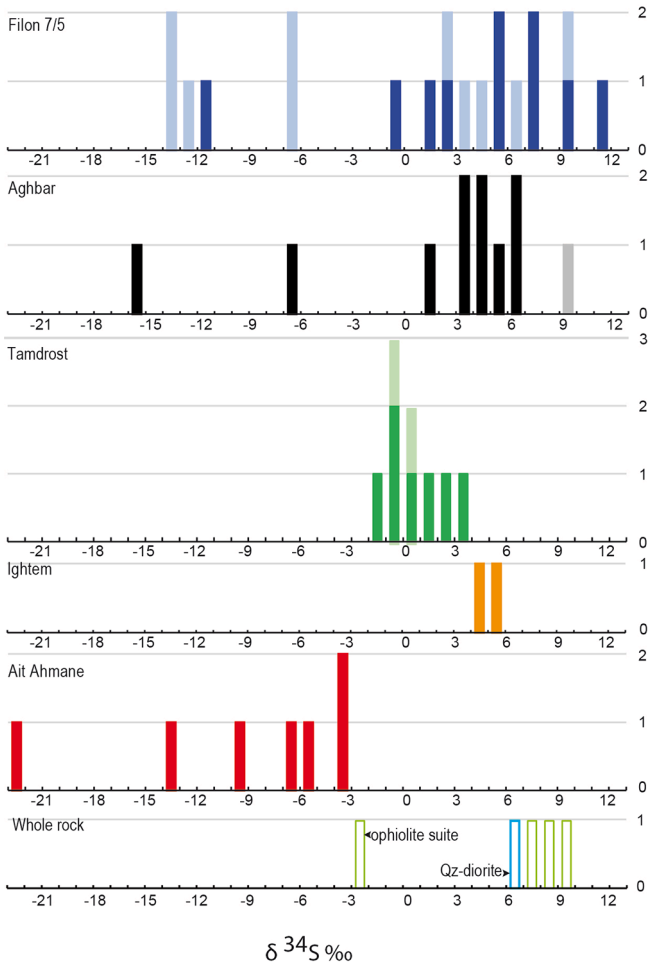

Fig. 8. Frecuency histogram showing S isotope compositions of ore phases and associated whole rocks. Arsenide data (this study) are shown in dark blue, black, green, orange and red colors, and epithermal sulphides (Levresse, 2001; Dolansky, 2007, Maacha et al., 2015) in light blue, gray and green colors.

linear data trends having different slopes. These features will form the basis for discussing two main aspects; the age of the ores and the source of ore lead. It is suggested here that the variable lead isotopes of Bou Azzer minerals reflect both in-situ decay and source mixing effects and their respective influence on data becomes ambiguous. This implies that in order to assign values of e.g. the average ore lead composition, the influence of these two processes must be clarified and this is best done by examining the total data set derived from the three studied ores.

In-situ decay and the age of ores: Not much is known about the tendency for common Ni and Co arsenides to incorporate U and Th in their lattices, a process governing an in-situ growth of the radiogenic lead isotopes. Yet, this tendency is probably marginal given the small ionic radius of the cations in relation to the large size of uranium and thorium ions. Arsenopyrite, on the other hand, is a phase known to mimic a true common lead mineral (i.e. having very low U/Pb and Th/Pb ratios). Nonetheless, one arsenopyrite analysis (#726) yielded exceptional high $^{206}Pb/^{204}Pb$ ratios (Table 3), whereas another arsenopyrite (#819) plots far away from other samples in the Pb-Pb diagrams. Arsenopyrite is a late phase of the main arsenide stage (stage II) and it is difficult to avoid the conclusion that the radiogenicity of arsenopyrite #726 is controlled by the presence of U-rich mineral inclusions. Such inclusions, dominated by brannerite (UTi_2O_6) have been recognized in e.g skutterudite from the Bou Azzer area (Dolansky, 2007, this study). Following this, it is reasonable to suggest that also other arsenides and sulfarsenides with elevated $^{206}Pb/^{204}Pb$ observed from Tamdrost and Aghbar obtained their radiogenic signature due to the presence of such inclusions. An in-situ U-Pb decay effect active ever since ore mineral formation will primarily affect the $^{206}Pb/^{204}Pb$ ratio and to a much less degree the $^{207}Pb/^{204}Pb$ ratio, implying that samples with a significant content of brannerite will be displaced along a flat slope towards the radiogenic end. The slope of the straight line, connecting mineral samples from different deposits in Fig. 5A, is not well constrained although an age in the 300–400 Ma time span is indicated. The age of ore formation remains a debated issue, and e.g. independent dating of brannerite and also molybdenite (Dolansky, 2007, Oberthür et al., 2009) have yielded $\leq$ 400 Ma ages which are comparable to the combined Aghbar and Tamdrost Pb-Pb age of 382 $\pm$ 56 Ma (this study). Other age estimates are close to 310 Ma (Oberthür et al., 2009). As it appears possible that mineralization ages vary across the district, we choose an intermediate value of 350 Ma for the purpose of setting an approximate age of district-scale ore formation. This model age corresponds to a slope value of 0.0542 (see the stippled lines in Fig. 5A) and the least radiogenic ore samples along this slope (i.e. those which are least affected by in-situ decay effects) have $^{206}Pb/^{204}Pb$ values between 17.9 and 18.0 and are defined by a group of four samples involving Aghbar #1026 skutterudite; Tamdrost #1551 löllingite; and Aït-Ahmane #999b and 2415 löllingite.

Mixing: The group of unradiogenic samples with comparatively constrained $^{206}Pb/^{204}Pb$ around 18 (Fig. 5A), which is defined by

Table 8
Major element contents (wt.%) in the selected country rocks from the Bou Azzer area.

	Al2O3	CaO	FeO	K2O	MgO	MnO	Na2O	TiO2
AgE-1	13.61	0.15	2.30	9.37	0.95	0.01	0.10	0.31
Tiddiline	12.24	1.28	5.21	0.69	0.67	0.06	5.78	0.88
WBW-2	15.00	2.84	3.36	2.36	1.66	0.07	3.50	0.42
Q-diorite	16.51	3.44	4.26	1.47	2.64	0.08	4.37	0.49
Qdi-6	18.48	3.29	5.13	0.44	3.88	0.12	7.06	0.60
Rodingite	15.54	6.02	5.25	1.49	3.13	0.61	4.29	0.48
B1, srp	0.92	0.08	6.02	0.09	34.01	0.09	0.02	0.01
OPH-DUN4	0.80	0.24	6.93	0.14	35.34	0.10	0.04	0.02
CPx-cumulate	10.10	8.60	9.83	0.23	15.46	0.21	0.85	0.27
OPH-CPx3	15.33	22.02	5.81	0.01	10.53	0.19	0.04	0.87
OPH-Ga2	18.25	8.54	8.84	0.90	4.97	0.18	2.83	0.73
OPH-CR1	7.06	0.05	7.46	0.02	9.89	0.31	0.02	0.04
Tpegm	15.77	0.22	0.67	8.74	0.20	0.01	2.40	0.05
TAK-2a	14.87	0.62	1.74	2.31	3.55	0.02	4.57	0.14
BW-3	13.46	0.35	5.04	3.15	1.91	0.06	1.39	0.58
FW-3	14.39	1.67	5.88	1.82	4.08	0.16	2.55	0.78
Trh40	13.41	0.22	3.02	7.38	0.43	0.03	0.12	0.29
T ORGN	18.25	0.28	5.26	6.00	0.88	0.01	0.12	0.64
DoIWB	1.20	22.67	0.86	0.31	15.43	0.18	0.17	0.05

Table 8B
Trace elements contents (ppm) in the selected country rocks from the Bou Azzer area.

	As	S	Co	Cr	Cu	Ni	Pb	Zn	Ag	Hf	Mo	Nb	Rb	Sr	Tl	U	Zr
AgE-1	28.3	X	4.2	172	2.4	13.7	1.7	6	X	2.99	1.8	7.5	114.67	19.58	0.53	2.71	104.3
Tiddiline	10.9	X	5.4	399	3.2	10.3	4	21	X	2.75	0.8	3.47	19.11	116.04	0.09	0.48	97.3
WBW-2	4.5	X	9.6	174	120.6	16.3	2.6	41	0.15	1.38	0.9	6.73	58.08	468.05	0.29	2.51	40.4
Q-diorite	11	X	13.3	135	535.7	13.3	3.9	75	1.23	0.37	0.8	4.48	30.84	472.46	0.12	0.62	4.3
Qdi-6	26.5	X	12.9	237	136	21.8	7.8	142	0.23	0.53	0.4	3.8	8.52	235.05	0.03	0.62	8.8
Rodingite	571.9	X	13	166	24.9	17.7	8.6	277	6.37	0.42	0.5	4.88	30.93	381.95	0.15	0.57	5.3
B1, srp	0.9	X	196.7	5638	19.4	2008.7	43.7	54	0.06	X	0.4	0.3	4.02	4.47	0.08	0.04	1.2
OPH-DUN4	5.6	0.1	129.8	3731	12.1	1932.6	2.9	44	0.51	0.07	0.7	0.17	2.03	14.81	0.09	0.44	2
CPx-cumulate	3	X	74	1680	3.5	152.9	3.3	100	X	0.61	0.3	0.89	3.3	203.85	0.03	0.2	21.8
OPH-CPx3	4	X	39.1	362	42.9	169.1	X	31	0.05	2.35	0.5	1.5	0.29	X	X	0.14	69.1
OPH-Ga2	2.6	X	32.3	1592	67.2	32.2	2.1	83	0.12	0.81	0.5	1.79	20.26	510.63	0.05	0.18	25.5
OPH-CR1	X	X	114.2	greater than20000	3.1	743.8	3.4	644	X	X	0.2	X	0.36	3.74	X	0.01	1
Tpegm	5.8	X	3	206	2.5	6.9	25.8	6	X	1.13	1.1	1.31	201.42	217.68	0.98	0.38	37.5
TAK-2a	34.7	X	13.5	437	4.9	172.3	1.5	18	0.06	0.3	1	0.6	41.9	208.16	0.13	0.3	8.1
BW-3	3	X	15.8	151	3.5	34.4	9.5	32	X	2.08	0.6	14.29	99.82	40.29	0.33	1.37	94.9
FW-3	5.1	X	31	224	8.1	106	4.5	96	0.29	2.67	0.6	7.55	39.5	125.19	0.18	0.65	104.3
Trh40	4	X	3.2	162	10	5.5	2.7	17	X	4.92	2	14.36	117.92	15.51	0.56	2.67	155.8
T ORGN	6.7	X	2.9	236	10.7	10.2	4	19	X	0.99	1.4	18.17	266.76	46.83	1.38	2.72	33.7
DoIWB	3.9	X	7.7	78	24.8	9.9	1.7	9	X	0.23	0.5	0.87	8.24	36.36	0.07	0.59	8

X: below detection limit.

Table 8C
Rare Earth Element contents (ppm) in the selected country rocks from the Bou Azzer area.

	La	Ce	Pr	Nd	Sm	Eu	Gd	Tb	Dy	Ho	Er	Tm	Yb	Y
AgE-1	37,13	46,71	5,82	19,56	3,01	0,5	2,51	0,4	2,54	0,49	1,52	0,24	1,6	13,07
Tiddiline	10,29	23,06	3,51	16,11	3,96	0,98	4,1	0,59	4	0,78	2,49	0,36	2,95	19,65
WBW-2	22,48	41,88	4,76	16,92	2,97	0,82	2,38	0,31	1,75	0,31	0,87	0,12	0,87	8,44
Q-diorite	9,04	19,51	2,7	11,98	2,62	0,87	2,33	0,33	1,74	0,32	0,85	0,12	0,69	8,11
Qdi-6	10,94	25,42	3,55	15,93	4,06	1,19	4,06	0,63	4,01	0,77	2,23	0,29	1,96	19,73
Rodingite	21,43	42,89	5,14	18,87	3,08	0,91	2,47	0,33	1,72	0,3	0,83	0,1	0,73	7,85
B1, srp	0,72	1,55	0,16	0,48	0,11	0,02	0,1	X	0,04	0,01	0,01	X	0,02	0,15
OPH-DUN4	0,85	1,11	0,13	0,47	0,1	0,03	0,12	0,02	0,12	0,03	0,08	0,02	0,07	0,65
CPx-cumulate	3,33	6,94	0,94	4,3	1,19	0,41	1,36	0,23	1,51	0,29	0,9	0,13	0,79	7,36
OPH-CPx3	4,97	12,32	1,87	9,54	3,19	0,64	4,36	0,77	5,53	1,18	3,76	0,55	3,92	32,53
OPH-Ga2	7,56	16,8	2,36	10,74	2,79	0,99	3,02	0,43	2,82	0,53	1,58	0,23	1,59	14,51
OPH-CR1	0,1	0,19	0,03	0,09	0,02	X	0,03	X	0,04	0,01	0,02	X	0,07	0,17
Tpegm	6,63	12,79	1,6	6,14	1,44	1,1	1,13	0,11	0,37	0,06	0,12	0,02	0,1	1,2
TAK-2a	0,99	1,62	0,23	1,05	0,28	0,13	0,43	0,06	0,38	0,07	0,19	0,03	0,17	2,13
BW-3	32,76	63,7	7,83	29,5	5,56	1	4,54	0,62	3,46	0,6	2,27	0,26	1,73	14,96
FW-3	8,93	25,05	2,93	12,47	3,21	0,92	3,33	0,6	4,16	0,82	2,37	0,35	2,44	19,51
Trh40	79,85	172,97	22,39	86,11	16,89	1,69	10,47	1,11	5,97	1,06	4,13	0,54	3,86	28,36
T ORGN	75,73	156,5	15,95	50,77	9,65	1,67	7,8	0,86	2,81	0,28	0,5	0,07	0,36	5,22
DoIWB	2,82	5,79	0,69	2,86	0,94	0,24	0,96	0,13	0,72	0,14	0,35	0,05	0,27	3,64

X: Under detection limit.

specimens from all three studied deposits, can be assumed not have been significantly influenced by in-situ decay processes. Hence, such values should represent essentially undisturbed ore lead signatures since ore formation; yet, there is a substantial variation of about 0.4 units in $^{207}Pb/^{204}Pb$ developed for these samples. A probable explanation to deviating $^{207}Pb/^{204}Pb$ values is an incomplete mixing mechanism involving ore sources with contrasting isotopic compositions. This finds support from the steep trends noted in the thorogenic diagram (Fig. 5B) for the considered group of samples. Such trends cannot result from the presence of brannerite inclusions (known to have very low Th/U values of about 0.0025 in the Bou Azzer area; Dolansky, 2007) as this would lead to markedly high $^{206}Pb/^{204}Pb$ ratios but not very elevated $^{208}Pb/^{204}Pb$ values. To sum up, the steeply aligned ^{207}Pb-^{206}Pb and ^{208}Pb-^{206}Pb isotope patterns at the low-radiogenic end of the data spectrum are probably an effect of mineralizing fluids acquiring lead from isotopically distinct sources.

Average ore lead: Given the noted ore lead isotope variability, and the existence of probable mixing effects, it is likely that no unique lead isotope signature represents the entire ore district. Rather, it is meaningful to try and define an average type of ore lead, and it was previously proposed that four unradiogenic samples could approximate the bulk ore lead in the district having a $^{206}Pb/^{204}Pb$ ratio of ca 17.9. The complementary $^{207}Pb/^{206}Pb$ and $^{208}Pb/^{206}Pb$ ratios can be derived from the relationships between the group of least radiogenic ore samples and the radiogenic samples displayed in Fig. 5. Leaving out five samples with extreme compositions (Tamdrost #1643/https://doi.org/10,1643/34 and Aghbar #819, 724 and 1026), the data of which will be shown not to reflect typical arsenide and sulfarsenide ore-forming conditions, the tentative flat trends aligning a large number of samples from Tamdrost and Aghbar, are actually passing near the field of unradiogenic data with $^{206}Pb/^{204}Pb$ close to 17.9. This adds support to the idea that the bulk of ore samples crystallized with this $^{206}Pb/^{204}Pb$ value; some of them (free from U-rich inclusions) are still reflecting this signature, whereas others (carrying inclusions) evolved with time and at the present time, their values define a flat slope in Fig. 5A. The intersection between the flat trend and the unradiogenic sample cluster define an average $^{207}Pb/^{204}Pb$ value of around 15.55. We are suggesting that the uranogenic 17.9/15.55 composition corresponds to a general situation where two or more end-components were thoroughly mixed prior to mineral deposition giving rise to an ore lead component typical of the Bou Azzer district (Fig. 5). By analogy, the appropriate (thorogenic) $^{208}Pb/^{204}Pb$ value, set by the group of samples with matching $^{206}Pb/^{204}Pb$ and $^{207}Pb/^{204}Pb$ values close to 17.9 and 15.55, is close to 38, or slightly lower (Fig. 5B). Hence, in further modelling, we will refer to an average type of ore lead with $^{206}Pb/^{204}Pb$, $^{207}Pb/^{204}Pb$ and $^{208}Pb/^{204}Pb$ at 17.9/15.55/37.9, respectively. By applying Stacey and Kramers (1975) two-stage model for terrestrial lead isotope evolution, this average lead composition yields a model age of about 440 Ma and a related my-value ($^{238}U/^{204}Pb$) of 9.58.

5.2. Source(s) of lead in ore fluids

Two samples can be distinguished as defining the previously outlined mixing array(s); Tamdrost #1643/10 (contains a marked proportion of an unradiogenic source; low in ^{207}Pb), and Aït-Ahmane #999 (contains a significant amount of a more radiogenic source; high in ^{207}Pb). Tentatively, these samples reflect a binary mixing process involving two isotopically, rather well-defined end-members existing at the approximate time (350 Ma) of ore formation. Although this is probably an oversimplification, their isotopic compositions can still be used to discuss the nature of rocks that delivered the lead component to the ores. Fig. 9 shows calculated lead isotope compositions of potential source rocks at 350 Ma and, with respect to a proposed mixing array, three rock types are relevant to discuss further; 1) an inferred basement, 2) ophiolites and 3) sedimentary rocks.

Basement-Pb: Two ore minerals, #819 arsenopyrite and #1643/10 löllingite, and some rocks have $^{206}Pb/^{204}Pb$ values less than 17 (Fig. 5A) that are isotopically less evolved than lead typically existing during Neoproterozoic or Devonian-Carboniferous times. Although a much older formation age cannot completely be ruled out, the favored explanation is that Hercynian tectonic processes led to an incorporation of a very significant (#1643/10) to significant (#819) basement component characterized by unradiogenic lead that has resided in an environment with very low Th/Pb and U/Pb ratios. The analyzed pegmatite (T-pegm) has an extremely low $^{206}Pb/^{204}Pb$ value of about 15.5 which argues for an old emplacement age. The lead in this rock is mostly contained in K-feldspar that is a comparatively lead-rich phase and also considered to be a common Pb mineral (with a very low U/Pb concentration ratio) that keeps its primary magmatic composition intact over time. Therefore, this rock type is an obvious supplier of a distinctly unradiogenic component to an evolving ore-forming fluid, and its extremely unradiogenic composition implies that this rock must have formed in the early Proterozoic. From this it is inferred that there are old basement rocks present in the Bou Azzer-El Graara inlier which contributed ore lead to the Ni-Co deposits. Tentatively, the analyzed orthogneiss (T-ORGN) is also early Proterozoic and may have formed from a similar magma source as the pegmatite, but its lead isotope composition changed moderately over time due to in-situ decay of uranium (and thorium) fixed in phases like biotite and amphibole. Supporting this is the ~ 1.8 Ga reference line drawn to connect the pegmatite and orthogneiss data points in Fig. 6A. Such an age is similar to detrital zircon ages obtained from sediments sampled in the same region (Bouougri et al., 2020; Lahna et al., 2020).

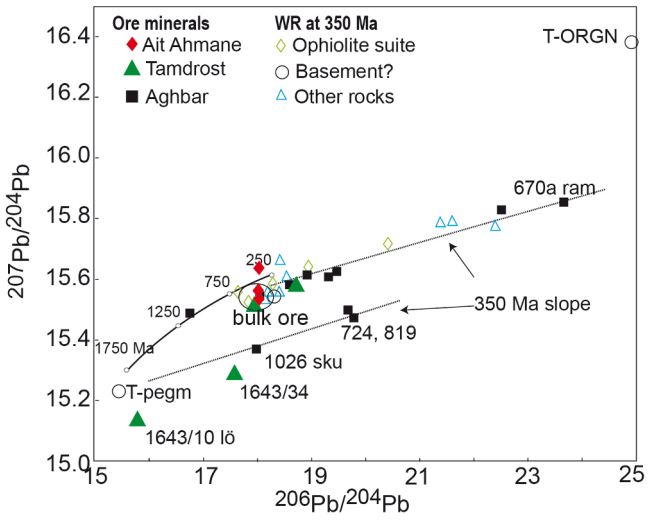

Fig. 9. A $^{207}Pb/^{204}Pb$ versus $^{206}Pb/^{204}Pb$ plot showing values representing the situation at the time of the inferred ore formation at t = 350 Ma. Ore mineral data correspond to the present-day ratios (cf. Table 1), whereas rock data are re-calculated to t = 350 Ma. The indicated ore signature defined by the least radiogenic ore data (encircled area) overlaps with the least radiogenic values of rocks of the ophiolite suite, and there are also other rock types sharing this isotopic signature. Part of the Stacey-Kramers (1975) two-stage curve is added as a reference.

Ophiolite-Pb: Whereas a basement component is probably not commonly available and therefore more rarely involved in ore-forming processes, the Upper Cryogenian ophiolite sequence of rocks is clearly spatially associated with Co-Ni ore deposits. Given that also a number of ophiolitic rocks have a lead isotope composition (at 350 Ma) that quite well matches the average ore lead composition (cf. Fig. 9) is a strong evidence for a genetic connection as well. Ultramafic rocks (such as dunites and pyroxenites) are quite low in lead (Faure, 1986), and possibly serpentinites that often are intimately associated with ore-bearing structures have been the dominant ophiolitic rock type supplying lead, as well as Co and Ni (Hajjar et al., 2021), to the ores. Qz-

diorite is another rock type with a common spatial relationship to ores. Noting that both analyzed samples of this type had an initial (350 Ma) Pb isotope composition that plots relatively close to "average" ore lead (Fig. 9), therefore this rock type may indeed have supplied part of the lead.

Sediment-Pb: As also the analyzed Tiddiline rock shows a good match with average ore lead as seen from a comparison (at t = 350 Ma) in both the ^{207}Pb-^{206}Pb (Fig. 9) and ^{208}Pb-^{206}Pb diagrams, clastic rocks should also be considered as a supplier of ore lead. Carbonates are reactive and prone to interact with invading hot fluids, but the details of this suggested process are not clear and the significance of the highly radiogenic lead isotope composition of the analyzed carbonate rock (DOL-WB, Table 4) remains obscure. It might also be briefly mentioned that there are some odd lead isotope compositions (with low ^{207}Pb in relation to the content of ^{206}Pb) recognized. For instance, three samples from Aghbar (# 724, 819 and 1026) may be interpreted as containing a significant old common Pb component, similar to that observed for the pegmatite (T-pegm), that controlled the composition attained during mineral deposition; in addition, these samples probably contain brannerite inclusions that over time (350 – 0 Ma interval) pushed the data points towards more radiogenic compositions (Fig. 5).

In summary, it is believed that ore-forming fluids have picked up lead from a range of source rocks with serpentinites and quartz-dioritic rocks as the main suppliers. Besides, basement rocks are likely to have supplied an unradiogenic component, and possibly sediments contributed a minor, more radiogenic (high in ^{207}Pb) type of lead.

5.3. Sources of Sr, Nd ore components

Source(s) of strontium in ore fluids: Sr isotope data of ore specimens are relatively few, but it seems that contrary to the Pb (and Nd) isotopes, quite homogeneous $^{87}Sr/^{86}Sr$ compositions of around 0.709–0.710 (Fig. 10, calculated for t_{ore} = 350 Ma) characterize the strontium contained in arsenides and carbonates. Contrary to the mineral phases, which have low Rb/Sr element ratios, some rocks show quite elevated Rb contents and since the Rb-Sr system is relatively susceptible to post-crystallization disturbances, back-calculated $^{87}Sr/^{86}Sr$ values, both to the time of rock crystallization and to the inferred ore formation (350 Ma), may become uncertain. This effect is normally insignificant for

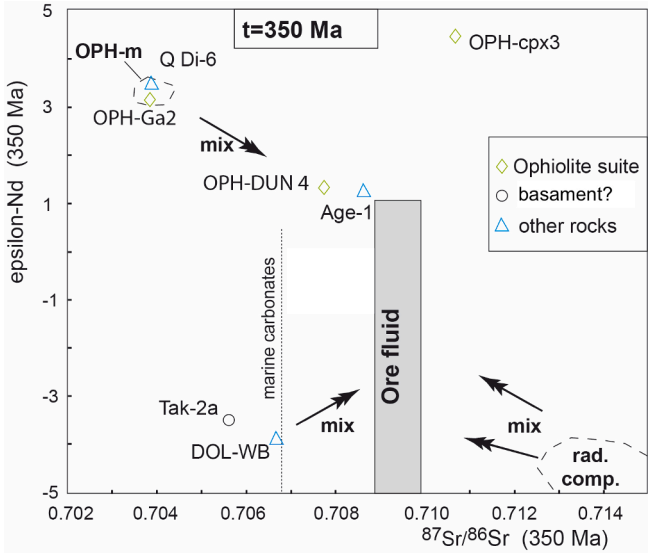

Fig. 10. An epsilon-Nd versus Sr plot based on rock data calculated at the time of the inferred ore formation (350 Ma). Available mineral data do not allow the Nd isotope character of the ore-forming solutions to be constrained, however, its Sr isotopic signature is indicated (grayish field). Added is also the Sr isotope composition of Carboniferous carbonate rocks (vertical stippled line).

mafic rocks, known to generally have low Rb/Sr concentration ratios, and therefore the spread in Sr isotope compositions (350 Ma) with values as low as 0.7038 for a gabbro and an extreme value above 0.712 for the analyzed serpentinite, is not expected. The elevated value for the serpentinite, featuring an unusually high Rb/Sr ratio (Table 5), may suggest interaction with crustal fluids as part of the serpentinization process close in time to the magma emplacement, but also e.g. a dunite and a clinopyroxenite have elevated ratios at t = 350 Ma.

Given the available results, only the analyzed gabbro and the quartz-diorite, with $^{87}Sr/^{86}Sr$ values of $\leq$ 0.704 at t = 350 Ma, have a strontium isotope composition typical for a rock of a mantle origin. Two hypotheses may be put forward to explain the $^{87}Sr/^{86}Sr$ values (t = 350 Ma) well above 0.705 for most mafic rocks; one of them is that crustal assimilation during magma generation introduced radiogenic strontium into most magmas. Another possibility, which is in line with the near-deposit location for several of the analyzed rocks and the identified radiogenic strontium in ore-forming fluids, is that evolved mineralizing fluids have interacted with juvenile mafic rocks ($^{87}Sr/^{86}Sr$ below 0.704). Irrespective of the mechanisms that controlled the strontium isotope signatures in rocks, the isotope range (0.709–0.710) indicated for the ultimate fluids depositing ore minerals is suggesting an isotopic exchange between mineralizing fluids and country rocks prior to ore deposition. It is noteworthy that the homogeneous ore strontium values imply that a relatively thorough mixing preceded ore formation. However, such an effect that equalizes contrasts in source end-member compositions is not indicated from lead isotope data. To overcome this apparent discrepancy, it may be that a single, relatively homogeneous source with a high concentration of strontium dominated ore-forming fluids and controlled their Sr isotopic composition.

Source(s) of neodymium in ore fluids: Due to the described problems related to analyses of ore minerals their corrected Nd isotope values, as shown in Fig. 7, are uncertain. More attention can be given to Nd isotope data provided for ore carbonates sampled in three areas across the Bou Azzer district (Oberthür et al., 2009). When calculated for an approximate ore formation age, these values (eps-Nd, t = 350 Ma) suggest that ore fluids carry neodymium of a highly variable composition, but dominantly with negative eps-Nd values (Fig. 7). Such values are not consistent with a pure origin from a mantle-derived source which is likely to have values near + 7 to + 8.

The Nd isotope data of the analyzed rocks in this study produce a scattered impression when present-day compositions are plotted (Fig. 7). Three ophiolite-type samples (dunite, OPH-cpx3 and the gabbro), the Qz-diorite and the andesitic tuff scatter around a reference line drawn for a 658 Ma age. These data indicate that certain samples may have originated from a magma source with an approximate + 4 eps-Nd value, i.e. not as deleted as expected from a pure mantle-derived melt. A logical implication is that crustal assimilation processes may have affected the magma-generating event leading to deposition of ophiolite-type rocks. Other rock types indicate generally even less positive eps-Nd values, i.e. a formation from a quite evolved magma source. Notably, some rocks (Tak-2a, BW-3, T-ORGN and T-pegm), several of them situated in the region close to the Bleida Far West occurrence (Fig. 1), have more CHUR-like or even enriched ƐNd values and their model ages are much older than their emplacement ages (Table 6). The high Nd model ages may be interpreted in two ways; either the rocks are Neoproterozoic and incorporated a very significant old basement component, or they represent truly early Proterozoic magmas. In the absence of new radiometric data, but irrespective of the preferred interpretation, the local existence of an old basement is nevertheless indicated.

Our interpretation of available data is that ophiolite-related rocks and certain crustal, felsic rocks were involved in the ore-forming processes at 350 Ma. Fig. 10 is a combined Nd-Sr diagram constructed to illustrate the situation at this time using Nd data for ore carbonates (Oberthür et al., 2009) and Sr data for ore phases and rocks (this study). From the available data, the shaded box constrains possible Nd and Sr isotope values for ore fluids, and clearly the ore fluid composition is not

consistent with an origin from a pure juvenile source with a depleted Sr and Nd isotope character. Thus, although ore fluids may have originated from a depleted source, equal to an ophiolite-related component (marked by ophiolite magma? in Fig. 7), it appears that other, isotopically contrasting and evolved sources are required to explain the range in the Sr-Nd isotopic signatures of ore fluids. The available depleted component may be reflected by the mantle-derived gabbro which will be shown to have a magmatic S isotope composition and hence may have escaped an (crustal) assimilation effect. Relatively few isotope data exist for crustal rocks and this inhibits the possibility to quantify crustal assimilation processes and to draw tentative mixing hyperbolas illustrating the possible interaction between different sources and ore fluids. Nonetheless, arrows are to Fig. 10 to simply illustrate that ore-forming fluids likely picked up Sr and Nd from both mantle-derived and crustal rocks in agreement with the conclusion drawn on basis of the lead isotope systematics.

5.4. Source (s) of sulphur in ore fluids

Like e.g. fluid inclusion and Pb isotope evidence, S isotope data of ore minerals give a complex impression (Fig. 8). Available data cover a range of deposits but neither relatively few data from base metal sulphides (Maacha et al., 2015, Dolansky, 2007) representing a late epithermal mineralization stage (Bouabdellah et al., 2016) nor a more exhaustive data set from the arsenide-sulfarsenide parageneses (this study) are conclusive. Basically, both data sets involve distinctly negative as well as positive values, and we are not able to see patterns relating obtained S isotope values to e.g. paragenetic stage, mineralogy or structural setting.

The S isotopic fractionation between arsenides/sulfarsenides and S species like H_2S is not easy to quantify because fractionation factors are not always known for pure phases and because metal substitution (Fe-Co-Ni) can take place (Liu et al., 2016). Generally, large isotopic differences are seen among analyzed samples, and the indicated relatively high hydrothermal temperatures (Dolansky, 2007) suggest that isotopic equilibrium is approached and that a fractionation between e.g. a sulfarsenide and H_2S will be limited and less than a few per mil. Therefore, an exact knowledge of mineral-dependent fractionation is considered less important and will not affect conclusions to be drawn.

Mineral deposition in the Bou Azzer area involved rare barite along with a massive presence of sulphides, arsenides and sulfarsenides, and this argues for a total dominance of reduced sulphur in ore-forming fluids. This in turn is suggesting that the dependence of S isotope data on changes in pH and fO_2 will not be very large. From this follows that an analyzed S isotope value for a sample will be similar to that of locally available, dissolved H_2S and also approximatively equal to the value of the total sulphur in solution (Ohmoto, 1972). In other words, the obtained (and variable) $\delta^{34}S$ values imply that the isotopic composition of locally available dissolved sulphur is highly heterogeneous.

The metals, in particular, Ni and Co are likely to have been derived from a magmatic source, e.g. the ophiolite suite of rocks, and magmatic sulphur has $\delta^{34}S$ values that cluster around zero per mil. Tamdrost has the simplest distribution with $\delta^{34}S$ data that cluster around zero and hence could reflect a component totally dominated by magmatic sulphur. On the other hand, magmatic sulphur alone cannot explain the isotopic patterns from other deposits in the ore district, as for instance the bulk of S isotope data from Filon 7/5 and Aghbar deposits are around + 6 ‰. Besides, the occasionally negative values found at Filon 7/5 and Aghbar, and the strongly negative values characterizing the Aït-Ahmane deposit cannot be reconciled with a simple magmatic origin of sulphur. Some input of locally/regionally available sedimentary sulphur into a magmatic-type fluid carrying nickel and cobalt seems inevitable. There are no data available that help delineate if TSR (thermochemical sulphate reduction) or BSR (bacterial sulphate reduction) processes, or a combination of both, were responsible for producing reduced sulphur of variable isotopic composition. The most negative values are probably best explained by BSR processes and there are e.g. scattered sedimentary country rocks, like pelitic schists and black shales, that are likely to contain organic material that could drive a bacterial reduction process.

Interestingly, the analyzed rocks, including four ophiolite-related rocks and one Qz-diorite, are also isotopically variable with one $\delta^{34}S$ value (-2.2 ‰) for a gabbro that could reflect an undisturbed mantle signature, whereas the remaining values are clearly positive in the range six to nine per mil. This range of data is suggesting that the S isotopic compositions of ultramafic rocks and the rodingite must have been modified during serpentinization-related, hydrothermal alteration, or that mafic magmas assimilated sedimentary material. More data are needed to further understanding of the variable ore mineral signatures, but one important contribution was probably from isotopically variable mafic to ultramafic rocks. On the other hand, at least the clearly negative ore mineral values seem to demand a direct input of locally available sedimentary sulphur to a magmatic fluid at depositional sites.

5.5. Crustal assimilation of ophiolite-forming magmas

The previous discussion, based on S, Sr and Nd isotope data, point out mafic ophiolite-type of rocks as the source of metals and that ore-forming fluids carry a sedimentary component. One way to bring these observations together is to argue that ore-forming fluids interacted with sedimentary units, but another option is that mafic rocks actually assimilated sedimentary material already during magma generation. A way to shed more light on this issue is to use the lead isotope data set, and Fig. 11 shows initial lead isotope compositions for the individual ophiolite-related and other rock magmas, back-calculated to a common emplacement age of 658 Ma. In the frame-work of the plumbotectonics model (Zartman and Doe, 1981), such compositions are apparently slightly variable with some samples defining a data cluster between a mantle component and an upper crustal component (M and UC, respectively in Fig. 11), whereas others are seemingly linearly aligned. The data cluster (OPH-m in Fig. 11) is interpreted to represent an originally fairly homogeneous juvenile, mantle-derived magma source that has assimilated variable amounts of crustal rocks. Tentatively, this

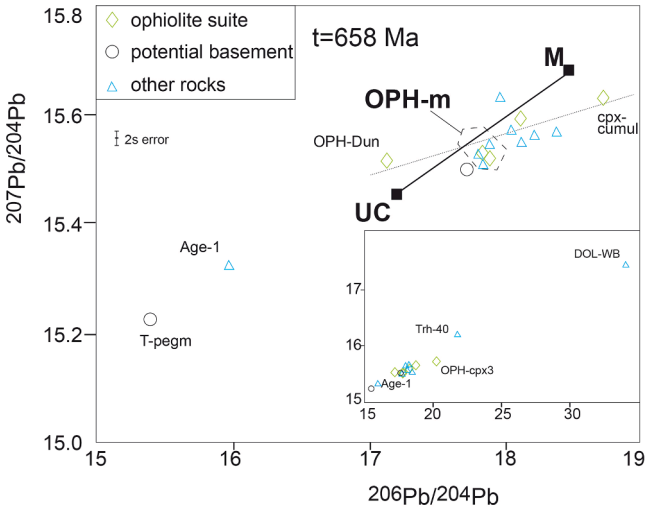

Fig. 11. A $^{207}Pb/^{204}Pb$ versus $^{206}Pb/^{204}Pb$ plot representing the situation at the time of ophiolite formation (at 658 Ma), with a complementary inset covering the more extreme isotopic compositions. The range of values for rocks of the ophiolite suite may indicate a variable contamination of the ophiolite magma (cf. the dotted line). Symbols M and UC stand for the approximative Pb isotope composition at t = 658 Ma of the mantle and upper crust, respectively. To illustrate the possible role of deep-seated (basement?) and more surficial contamination (dolomite?) of the ophiolite -forming magma, calculated isotope values of other rock types (at 658 Ma) are also shown. However, the latter are uncertain given that certain rocks are believed to be younger than 658 Ma.

data cluster represents the lead isotope compositions of all analyzed ophiolite-rocks at the time of their emplacement. Nonetheless, certain mafic samples apparently plot outside this cluster and either this discrepancy is due to post-crystallization processes whereby minor amounts of lead or uranium was added, or lost, to the rock system. Such a process would compromise the back-calculation procedure that is based on a closed-system behavior, and instead of creating a narrow data cluster in the used diagram type, certain data would fall along a 658 Ma isochron (indicated to the dotted trend line in Fig. 11). Alternatively, the generalized crustal component depicted in the plumbotectonics model is not appropriate to consider. Instead, a more complex crustal assimilation affecting a mafic magma chamber, involving pre-658 Ma rocks in the area, may be a more viable process. The latter option finds some support from the overall pattern in Fig. 11 where some country rocks, e.g. Trh-40 (rhyolite) and the pegmatite (T-pegm), have calculated isotopic compositions at 658 Ma which plot at the extreme ends of the linear trend line, and thereby may comprise tentative assimilants into a magma chamber. To conclude, the inferred crustal assimilation event can explain why e.g. published Nd isotope data of ophiolites and associated rocks (Ikenne et al., 2020) are not typical for a pure, juvenile mantle component and why isotopically heavy sulphur is characterizing most ophiolites (this study).

5.6. Ore-forming model

A range of investigations have been carried out on several Co-Ni ores of the Bou Azzer area. Such data together with new results from this study enable the construction of an updated model with emphasis on isotopic constraints on the timing and nature of ore-forming processes.

Timing: Available geochronological and field data are offering various possible ages of mineralization. Generally, radiometric ages may, except for representing real ore-forming events, signify e.g. hydrothermal alteration, late veining and isotopic resetting. Ikenne et al. (2020) did not rule out the possibility of a primary Pan-African mineralization event followed by remobilization of metals during Hercynian events. Supporting a temporal relationship between Pan-African and mineralization events is the structural setting where the main orebodies are located along transcurrent sinistral faults belonging to the ultimate Pan-African phase, active between 615 and 580 Ma ago. However, no published radiometric dating of ore components supports a Pan-African connection, and crosscutting and offsetting relationships imply that orebodies postdate the serpentinization (Fanlo et al., 2015) and the structures of the major Pan-African tectonic phase (Leblanc and Billaud, 1982).

Basically, the geochronological evidence suggests two age modes; an older mode between ca. 380 and 355 Ma is defined by U-Pb brannerite ages at Filon 7/5 (Dolansky, 2007), which represent "chemical dates" obtained by using an electron microprobe. Similar ages, $\leq$400 Ma, were obtained from Pb-Pb relationships defined by ore minerals from Aghbar and Tamdrost (this study), and from Ar-Ar dating of muscovite from a barren quartz vein at Tamdrost (Levresse, 2001). Also, Re-Os molybdenite ages from Filon 7 and Aghbar fall in the 400–350 Ma interval (Oberthür et al., 2009). However, it must be recalled that although this system usually yields robust age information the presented dates are model ages that rely on certain assumptions, and Oberthür et al. (2009) and Ikenne et al. (2020) raised doubts about their relevance. A younger age mode at ~ 310 Ma is indicated by laser ablation, ICPMS U-Pb brannerite ages of Filon 7 samples (Oberthür et al., 2009), and similar ages were obtained from ore carbonates sampled in three different areas of the district using the Sm-Nd method (Oberthür et al., 2009). However, ages significantly younger than about 300 Ma, e.g. ca. 220 Ma Ar-Ar muscovite ages at Tamdrost (Levresse, 2001), 260 Ma, or lower, U-Pb ages of altered brannerite from Filon 7/5 (Dolansky, 2007, Oberthür et al., 2009), might reflect later over-printing events that did not involve any new addition of metals.

Apparently, brannerite is a key mineral for putting age constraints on ore formation, but its high U content makes this phase susceptible for post-crystallization lead loss as also seen in partly discordant U-Pb data defining a lower intercept age at 65 Ma (Oberthür et al., 2009). It is viable that post-crystallization processes could also explain why there is a bimodal brannerite U-Pb age distribution. One possibility is that analyzed brannerite clusters (Oberthür et al., 2009) have suffered a complete lead loss during Hercynian peak-metamorphism, and that the obtained 310 Ma date is a reset age. If so, 385–350 Ma brannerite ages (Dolansky, 2007) of unaltered brannerite inclusions in skutterudite are the best estimate of brannerite crystallization, and by inference ore formation. Also, similar $\leq$ 400 Ma Pb-Pb dates of arsenides (this study), essentially controlled by coeval brannerite inclusions, may be significant if arsenide grains have acted as a shield preventing the Pb-Pb system of brannerite to become disturbed by later hydrothermal-tectonic events. Altogether, radiometric evidences do not allow any tight age constraint to be set on ore formation. Probably, the 400–300 Ma period witnessed a series of tectonic and hydrothermal events, and given the variability in e.g. isotopic and fluid inclusion results it seems feasible that several episodes of ore mineral deposition occurred in this time interval.

Ore-forming scenario: Our working hypothesis is that the primary introduction of metals took place during Devonian-Carboniferous, district-scale events that reactivated old Pan-African tectonic structures as a result of N-S shortening (Gasquet et al., 2005). An episode of ore deposition may have involved repeated re-activation of old faults along with concurrent vein formation and initiation of hydrothermal fluid flow. Lead isotope data of ore minerals (this study) point out ophiolite-related rocks, e.g. serpentinites, and also quartz-diorites as major sources of metals. Both rock types have a strong spatial relationship to ore bodies and show isotopic signatures at the proposed average (350 Ma) time of ore formation that match the inferred lead isotope composition of the bulk ore. Serpentinites are also often showing dissolution textures as a result of fluid interaction (Hajjar et al., 2021) which argue for a direct involvement in ore formation. Probably, competence contrasts between serpentinites and surrounding wall rocks have governed the development of weakness zones (e.g. fault zones; Tourneur et al., 2021) that have acted as conduits for mineralizing fluids.

It is likely that tectonic activity triggered the percolation of fluids along shears and faults across a large area. Such fluids probably interacted with mafic magmatic rocks, thereby leaching nickel and cobalt, but substantial amounts of other elements were also picked from country rocks. Following earlier suggestions (En-Naciri, 1995, En-Naciri et al., 1997, Dolansky, 2007), ore fluids comprised reduced brines that became more oxidized at later stages. This view is basically consistent with hydrogen and oxygen isotope evidence (Dolansky, 2007, Maacha et al., 2015) which were interpreted to support the presence of hot, saline fluids of magmatic origin, and that cooler, dilute meteoric fluids subsequently entered mineralization sites. The complex picture arising from fluid inclusion studies is also in agreement with fluid mixing and associated changes in e.g. temperature and salinity. Fluids of meteoric origin that progressively invaded ore sites, and perhaps also triggered mineral precipitation, may have released reduced sulphur from e.g. pelitic schists that locally cap the ophiolite sequence. Carbonate rocks are reactive and locally abundant and the Sr isotope composition of an analyzed single sample appears to have been modified by percolating fluids suggesting that e.g. strontium and calcium were released from carbonates and picked up by percolating hydrothermal fluids.

Obviously, fluids that have experienced this geologic history could have passed, and interacted with, a range of rocks having different isotopic signatures before reaching a final site of ore deposition. Partly strongly negative εNd values of analyzed carbonates (Oberthür et al., 2009; this study), indicate a systematic variation with geographical location suggesting that at certain sites ore-forming fluids must have interacted to a significant degree with an old, enriched source, as also indicated e.g. by an early Proterozoic lead isotope signature for a löllingite (#1643/10) from Tamdrost. When summarizing field and other data, a magmatic (ophiolitic) source of e.g. sulphur, lead and

strontium probably was important at all sites, but ore elements were released also from various country rocks and this created heterogeneous ore isotope characteristics. Not least the suggested assimilation/alteration history for the ophiolitic-type rocks, that led to isotopic heterogeneities, played a role in creating partly erratic analytical results.

6. Conclusions

- Overall, new data from the present study, and other evidence, support Devonian-Carboniferous mineralization events operating on a large regional scale as a response to N-S shortening. Probably, the features of different deposits are the ultimate result of multi-episodic ore-forming events in connection with repeated re-activation of old faults along with concurrent vein formation and initiation of hydrothermal fluid flow.

- Although derived from the mantle, the ophiolite-related rocks do not exhibit typical mantle isotopic signatures. This might be explained by assimilation processes where crustal material may have been incorporated during crystallization of discrete magmas.

- It is suggested that ophiolites of a mantle origin rocks have been the main supplier of ore elements. Yet, Pb, Sr, Nd and S isotope data generate a quite consistent picture where ore fluids have scavenged elements from a number of isotopically different crustal sources including both inferred basement lithologies and sedimentary rocks.

- The presence of minute, coeval brannerite inclusions in arsenides and sulfarsenides excerpts a strong control on their lead and neodymium isotope behavior.

- Pb isotope results suggest that certain of the studied felsic rocks represent early Proterozoic lithologies. Based on old Nd model ages, it is possible that also additional rocks may be much older than hitherto believed; an alternative interpretation is that these rocks have incorporated significant amounts of old basement components. New radiometric dating is required in order to shed further light on this issue.

Declaration of Competing Interest

The authors declare that they have no known competing financial interests or personal relationships that could have appeared to influence the work reported in this paper.

Acknowledgements

The authors greatly acknowledge the geological survey of CTT-Bou Azzer mine for facilitating our geological field campaigns and specially to Clemente Recio (University of Salamanca) for his invaluable help to IS during the development of the analytical procedure to measure S isotope compositions from the minor amounts of S extracted from arsenides and sulfarsenides. Authors would like to acknowledge the use of Servicio General de Apoyo a la Investigación-SAI, Universidad de Zaragoza. This research was financially supported by the Spanish project RTI2018- 099157-A-I00 granted by the "Ministerio de Ciencia, Innovación y Universidades". The Swedish Research Council (infrastructure grant: Dnr. 2017-00671) is thanked for financial support to the Vegacenter national laboratory. This is Vegacenter publication number 124

References

Ahmed, A.H., Arai, S., Ikenne, M., 2009. Mineralogy and paragenesis of the Co-Ni arsenide ores of Bou Azzer, Anti-Atlas, Morocco. Econ. Geol. 104 (2), 249–266.

Álvaro, J.J., Benziane, F., Thomas, R., Walsh, G.J., Yazidi, A., 2014. Neoproterozoic-Cambrian stratigraphic framework of the Anti-Atlas and Ouzellagh promontory (High Atlas), Morocco. J. Afr. Earth Sci. 98, 19–33.

Asmerom, Y., Jacobsen, S.B., Knoll, A.H., Butterfield, N.J., Swett, K., 1991. Strontium isotopic variations of Neoproterozoic seawater: Implications for crustal evolution. Geochim. Cosmochim. Acta 55 (10), 2883–2894.

Blein, O., Baudin, T., Chèvremont, P., Soulaimani, A., Admou, H., Gasquet, P., Cocherie, A., Egal, E., Youbi, N., Razin, P., Bouabdelli, M., Gombert, P., 2014. Geochronological constraints on the polycyclic magmatism in the Bou Azzer-El Graara inlier (Central Anti-Atlas Morocco). J. Afr. Earth Sci. 99, 287–306.

Bouabdellah, M., Maacha, L., Levresse, G., Saddiqi, O., 2016. The Bou Azzer Co–Ni–Fe–As (±Au ± Ag) District of Central Anti-Atlas (Morocco): A Long-Lived Late Hercynian to Triassic Magmatic-Hydrothermal to Low-Sulphidation Epithermal System. In: Bouabdellah, M., Slack, F.J. (Eds.), Mineral Deposits of North Africa. Springer International Publishing, pp. 229–247.

Bouougri, E.H., Lahna, A.A., Tassinari, C.C.G., Basei, M.A.S., Youbi, N., Admou, H., Saquaque, A., Boumehdi, M.A., Maacha, L., 2020. Time constraints on early Tonian Rifting and Cryogenian Arc terrane-continent convergence along the northern margin of the West African craton: insights from SHRIMP and LA-ICP-MS zircon geochronology in the Pan-African Anti-Atlas belt (Morocco). Gondwana Res. 85, 169–188.

Canfield, D.E., Raiswell, R., Westrich, J.T., Reaves, C.M., Berner, R.A., 1986. The use of chromium reduction in the analysis of reduced inorganic sulfur in sediments and shales. Chem. Geol. 54 (1-2), 149–155.

Clauer, N., 1976. Géochimie isotopique du strontium des milieux sédimentaires Application à la géochronologie du craton ouest africain: Thése Doct. Etat, Sci. Géol. Univ. Strasbourg, 45, 256 p.

Coleman, M.L., Moore, M.P., 1978. Direct reduction of sulfates to sulfur dioxide for isotopic analysis. Anal. Chem. 50, 1594–1595.

D'Lemos, R.S., Inglis, J.D., Samson, S.D., 2006. A newly discovered orogenic event in Morocco: neoproterozoic ages for supposed Eburnean basement of the Bou Azzer inlier, Anti-Atlas Mountains. Precambr. Res. 147 (1–2), 65–78.

Dolansky, L.M., 2007. Controls on the genesis of hydrothermal cobalt mineralization: insights from the mineralogy and geochemistry of the Bou Azzer deposits, Morocco. McGill University, Montreal, Canada, p. 162. Unpublished Master Thesis.

El Ghorfi, M., 2006. Etude géochimique et métallogenique des métaux précieux (or, argent et platinoïdes) associes aux minéralisations à Co, Ni, Cr de Bou Azzer-El Graara, et dans la série de Bleida Far West, Anti-Atlas, Maroc. Cadi Ayyad University, Marrakech, Morocco, p. 256 p.. PhD thesis.

El Hadi, H., Simancas, J.F., Martínez-Poyatos, D., Azor, A., Tahiri, A., Montero, P., Fanning, C.M., Bea, F., González-Lodeiro, F., 2010. Structural and geochronological constraints on the evolution of the Bou Azzer Neoproterozoic ophiolite (Anti-Atlas, Morocco). Precambr. Res. 182 (1-2), 1–14.

En-Naciri, A., 1995. Contribution 'a l'étude du district 'a Co., As (Ni, Au, Ag) de Bou Azzer. Anti- Atlas (Maroc) Données minéralogiques et géochimiques. Universíe d'Orléans, France, p. 245. PhD thesis.

En-Naciri, A., Barbanson, L., Touray, J.C., 1997. Brine inclusions from the Co-As (Au) Bou Azzer district, Anti-Atlas, Morocco. Econ. Geol. 92, 360–367.

Essarraj, S., Boiron, M.-C., Cathelineau, M., Banks, D.A., Benharref, M., 2005. Penetration of surface-evaporated brines into the Proterozoic basement and deposition of Co and Ag at Bou Azzer (Morocco): evidence from fluid inclusions. J. African Earth Sc. 41 (1-2), 25–39.

Fanlo, I., Gervilla, F., Colas, V., Subías, I., 2015. Zn-, Mn-, Co-enriched chromian spinels from the Bou-Azzer mining district (Morocco): constraints on their relationship with the mineralizing process. Ore Geol. Rev. 71, 82–98.

Faure, G., 1986. Principles of isotope geology, 2nd edition. John Wiley and Sons.

Gasquet, D., Levresse, G., Cheilletz, A., Azizi-Samir, M.R., Mouttaqi, A., 2005. Contribution to a geodynamic reconstruction of the Anti-Atlas (Morocco) during Pan-African times with the emphasis on inversion tectonics and metallogenic activity at the Precambrian-Cambrian transition. Precambr. Res. 140 (3-4), 157–182.

Gervilla, F., Fanlo, I., Colas, V., Subias, I., 2012. Mineral compositions and phase relations of Ni–Co–Fe arsenide ores from the Aghbar mine, Bou Azzer, Morocco. Can. Mineral. 50 (2), 447–470.

Hajjar, Z., Gervilla, F., Fanlo, I., Jiménez, J.-M., Ilmen, S., 2021. Formation of serpentinite-hosted, Fe-rich arsenide ores at the latest stage of mineralization of the Bou-Azzer mining district (Morocco). Ore Geol. Rev. 128, 103926. https://doi.org/10.1016/j.oregeorev.2020.103926.

Hall, G.E.M., Pelchat, J.-C., Loop, J., 1988. Separation and recovery of various sulfur species in sedimentary rocks for stable sulfur isotopic determination. Chem. Geol. 67, 35–45.

Hefferan, K., Soulaimani, A., Samson, S.D., Admou, H., Inglis, J., Saquaque, A., Latifa, C., Heywood, N., 2014. A reconsideration of Pan African orogenic cycle in the Anti-Atlas Mountains, Morocco. J. Afr. Earth Sci. 98, 34–46.

Ikenne, M., Souhassou, M., Saintilan, N.J., Karfal, A., El Hassani, A., Moundi, Y., Ousbih, M., Ezzghoudi, M., Zouhir, M., Maacha, L., 2020. Cobalt-Nickel-Copper arsenide, sulpharsenide and sulphide mineralisation in the Bou Azzer window, Anti-Atlas, Morocco: One century of multi-disciplinary and geological investigations, mineral exploration and mining. Geological Soc., London, Spec. Publ. 502. https://doi. org/10.1144/SP502-2019-132.

Inglis, J.D., Samson, S., D'Lemos, R.S., Admou, H., 2003. Timing of regional greenschist facies deformation in the Bou Azzer Inlier, Anti-Atlas: U–Pb constraints from syn-tectonic intrusions. First meeting of IGCP 485, El Jadida, Morocco, pp. 40–42.

Inglis, J.D., MacLean, J.S., Samson, S.D., D'Lemos, R.S., Admou, H., Hefferan, K., 2004. A precise U– Pb zircon age for the Bleida granodiorite, Anti-Atlas, Morocco: implications for the timing of deformation and terrane assembly in the eastern Anti-Atlas. J. Afr. Earth Sci. 39, 277–283.

Lahna, A.A., Youbi, N., Tassinari, C.C.G., Basei, M.A.S., Ernst, R.E., Chaib, L., Barzouk, A., Mata, J., Gärtner, A., Admou, H., Boumehdi, M.A., Söderlund, U., Bensalah, M.K., Bodinier, J.-L., Maacha, L., Bekker, A., 2020. Revised stratigraphic framework, for the lower Anti-Atlas Supergroup based on U-Pb geochronology of magmatic and detrital zircons (Zenaga and Bou Azzer-El Graara inliers, Anti-Atlas Belt, Morocco. J. Afr. Earth Sci. 171, 103946. https://doi.org/10.1016/j.jafrearsci.2020.103946.

Lasobras, E., 2012. Composición mineral y relaciones de fase de los arseniuros de Co- Fe-Ni del yacimiento de Aït-Ahmane (Bou-Azzer, Marruecos). Diferencias con otros depósitos. TFM. Universidad de Zaragoza, Spain, p. 53.

Lázaro, M., 2012. Mecanismos de reequilibrio mineral en arseniuros de Co-Fe-Ni en Tamdrost (Bou Azzer, Marruecos). TFM. Universidad de Zaragoza, Spain, p. 53.

Leblanc, M., 1975. Ophiolites précambriennes et gîtes arséniés de Cobalt (Bou Azzer. Maroc). PhD Thesis. Univ, Paris VI, France, p. 329.

Leblanc, M., 1981. The late Proterozoic ophiolites of Bou Azzer (Morocco): evidence for Pan-African plate tectonics. In: Kröner, A. (Ed.), Precambrian plate tectonics. Elsevier Amsterdam, pp. 451–455.

Leblanc, M., Billaud, P., 1982. Cobalt arsenide orebodies related to an Upper Proterozoic ophiolite: Bou Azzer (Morocco). Econ. Geol. 77 (1), 162–175.

Levresse, G., 2001. Contribution à Íetablissement d'un modèle génétique des gisements d'Imiter (Ag-Hg), Bou Madine (Pb-Zn-Cu-Ag-Au) et Bou Azzer (Co-Ni-As-Ag-Au) dans l'Anti-Atlas marocain. CRPG-CNRS, Nancy, France, p. 191. Ph.D. thesis.

Liu, S., Li, Y., Gong, H., Chen, C., Liu, J., Shi, Y., 2016. Frist-principles calculations of sulphur isotope fractionation in MX2 minerals, with M=Fe Co, Ni and X2=AsS. SbS. Chem. Geol. 441, 204–211.

Maacha, L., 2013. Etude métallogéniques et géophysiques des minéralisations cobaltiféres et cupriféres de Bou-Azzer El Graara Anti Atlas Maroc (Tome 1). Cadi Ayyad University, Marrakech, Morocco, p. 344. PhD Thesis.

Maacha, L., El Ghorfi, M., En-Naciri, A., Sadiqqi, O., Soulaimani, A., Alansari, A., Bhilisse, M., 2015. Nouvelles données isotopiques et d'inclusions fluides des minéralisations cobaltiféres de Bou Azzer. Apport à la géologie économique de la boutonnière. (Anti-Atlas central, Maroc). Notes et mém. Serv. Géol. Maroc 579, 133–139.

Mrini, Z., 1993. Chronologie (Rb–Sr, U-Pb), traçage isotopique (Sr–Nd-Pb) des sources des roches Magmatiques éburnéennes, panafricaines et hercyniennes du Maroc. Cadi Ayad University, Marrakech, p. 227. PhD thesis.

Naidoo, D.D., Bloomer, S.H., Saquaque, A., Hefferan, K., 1991. Geochemistry and significance of metavolcanic rocks from the Bou-Azzer-El Graara ophiolite (Morocco). Precambr. Res. 53 (1-2), 79–97.

Oberthür, T., Melcher, F., Henjes-Kunst, F., Gerdes, A., Stein, H., Zimmerman, A., El Ghorfi, M., 2009. Hercynian age of the cobalt-nickel-arsenide-(gold) ores, Bou Azzer, Anti-Atlas, Morocco: Re-Os, Sm-Nd, and U-Pb age determinations. Econ. Geol. 104 (7), 1065–1079.

Ohmoto, H., 1972. Systematics of sulfur and carbon isotopes in hydrothermal ore deposits. Econ. Geol. 65 (5), 551–578.

Pin, C., Zalduegui, J.S., 1997. Sequential separation of light rare-earth elements, thorium and uranium by miniaturized extraction chromatography: application to isotopic analyses of silicate rocks. Anal. Chim. Acta 339 (1-2), 79–89.

Recio, C., Fallick, A.E., Ugidos, J.M., 1991. Sulfur isotope systematics of granitoids and associated rocks from the Avila-La Alberca area (western Sistema Central, Spain). Rev. Soc. Geol. España 4, 371–381.

Saquaque, A., Benharref, M., Abia, H., Mrini, Z., Reuber, I., Karson, J.A., 1992. Evidence for a Panafrican volcanic arc and wrench fault tectonics in the Jbel Saghro, Anti-Atlas, Morocco. Geologische Rundschau 81 (1), 1–13.

Samson, S.D., Inglis, J.D., D'Lemos, R.S., Admou, H., Blichert-Toft, J., Hefferan, K., 2004. Geochronological, geochemical, and Nd-Hf isotopic constraints on the origin of Neoproterozoic plagiogranites in the Tasriwine ophiolite, Anti-Atlas orogeny, Morocco. Precambr. Res. 135, 133–147.

Stacey, J.S., Kramers, J.D., 1975. Approximation of terrestrial lead isotope evolution by a two-stage model. Earth Planet. Sci. Lett. 26 (2), 207–221.

Stueber, A.M., Goles, G.G., 1967. Abundances of Na, Mn, Cr, Sc and Co in ultramafic rocks. Geochim. Cosmochim. Acta 31, 75–93.

Soulaimani, A., Ouanaimi, H., Saddiqi, O., Baidder, L., Michard, A., 2018. The Anti-Atlas Pan-African Belt (Morocco): overview and pending questions. C. R. Geosci. 350 (6), 279–288.

Todt, W., Cliff, R.A., Hanser, A., Hofmann, A.W., 1996. Evaluation of a ^{202}Pb-^{205}Pb double spike for high-precision lead isotope analysis, in Earth Processes: Reading the Isotopic Code. In: Basu, A., Hart, S.R. (eds), Geophys. Monogr. Ser. AGU, Washington, D.C. 95, 429–437.

Tourneur, E., Chauvet, A.m Kouzmanov, K., Tuduri, J., Paquez, C., Sizaret, S., Darfal, A., Moundi, Y., El Hassani, A. 2021. Co-Ni-arsenide minealisation in the Bou Azzer district (Anti-Atlas, Morocco): Genetic model and tectonic implications. Ore Geol. Rev. 10.1016/j.oregeorev.2021.104128.

Triantafyllou, A., Berger, J., Baele, J.-M., Bruguier, O., Diot, H., Ennih, N., Monnier, C., Plissart, G., Vandycke, S., Watlet, A., 2018. Intra-oceanic arc growth driven by magmatic and tectonic processes recorded in the Neoproterozoic Bougmane arc complex (Anti-Atlas, Morocco). Precambr. Res. 304, 39–63.

Triantafyllou, A., Berger, J., Baele, J.-M., Mattielli, N., Ducea, M.N., Sterckx, S., Samson, S., Hodel, F., Ennih, N., 2020. Episodic magmatism during the growth of a Neoproterozoic oceanic arc (Anti-Atlas, Morocco). Precambr. Res. 339, 105610. https://doi.org/10.1016/j.precamres.2020.105610.

U.S. Geological Survey, 2013. Mineral commodity summaries 2013. U.S. Geological Survey, p. 198.

Zartman, R.E., Doe, B.R., 1981. Plumbotectonics – the Model. Techtonophysics 75 (1-2), 135–162.